

Seismic Characterization of Slope Deposits of Carbonate Shelf Margins

By:
William Garland Mynatt

Submitted to the graduate degree program in Geology and the Graduate Faculty of the
University of Kansas in partial fulfillment of the requirements
for the degree of Master of Science.

Chair: Dr. Eugene C. Rankey

Dr. Diane L. Kamola

Dr. George P. Tsoflias

Date Defended: October 15, 2020

The thesis committee for William Mynatt certifies that this is the approved version of the following thesis:

Seismic Characterization of Slope Deposits of Carbonate Shelf Margins

Chair: Dr. Eugene C. Rankey

Date Approved: December 18, 2020

Abstract

Seismic data are essential to understanding subsurface geology, but the marked geological and architectural variability of carbonate strata relative to seismic resolution can hinder accurate interpretation. To test the hypothesis that lateral variations in facies and petrophysical properties produce observable change in the seismic response of carbonate shelf margins, a suite of geological scenarios based on real-world outcrop, well, and high-resolution seismic data forms the basis for seismic models that systematically isolate geological variables. Eleven geological scenarios that changed the presence and location of high- and low-impedance intervals or differing stratal geometries were modeled seismically at three different frequencies. Results demonstrate that 1) lateral changes in facies and petrophysical properties, even when below the limits of seismic resolution, subtly alter the amplitude, period, and geometry of reflectors; and 2) time lines such as sequence boundaries may, or may not, follow reflectors. These subtle changes, applied to real-world seismic data, provide means of constraining plausible geological interpretations based on reflector character.

Acknowledgements

I would like to thank Dr. Eugene Rankey, for serving as my advisor and mentor during my time at the University of Kansas and for making me the geologist I am today. I would also like to thank Dr. Diane Kamola for serving on my committee and for her comments to improve the quality of this work. I would like to thank Dr. George Tsoflias for serving on my committee, and for his comments and thoughts to improve the quality of this work. I would like to thank Tom Neal, for his advice and support both as a friend and as a colleague. I would also like to thank the rest of the Kansas Interdisciplinary Carbonate Consortium (KICC) research group for their friendship: Arwin Dobber, Adam Lane, and Michelle Mary. I would like to thank the Applebee's Crew for their friendship and mental and emotional support in the final year of my time in Kansas: Ethan Doerger, Caroline Nazworth Doerger, Julie Sophis, and Craig Bennett. I would also like to thank my family for the sacrifices they made for me to get here, and for their support throughout my academic career. I would like to thank Dr. Jim Puckette from Oklahoma State University for inspiring me to pursue a career in geology. Finally, I would like to thank my girlfriend, Courtney Gard, for her continuous emotional and mental support throughout my final, unconventional, year of school. Support for this project came from the Kansas Interdisciplinary Carbonate Consortium and the University of Kansas Geology Department.

Table of Contents

Abstract.....	iii
Acknowledgements.....	iv
Table of Contents.....	v
Introduction.....	1
Background.....	4
Physical Model Design	4
Petrophysical Properties and Seismic Modeling.....	8
Results- Seismic Models.....	9
Models of Slope Deposits of an Aggrading Carbonate Shelf.....	10
Observations	10
Interpretation.....	11
Models of Slope Deposits of Low-Relief, Interfingering Shelf and Basinal Strata.....	13
Observations	13
Interpretation.....	13
Models of Slope Deposits of Prograding Carbonate Margins	14
Observations	14
Interpretations	16
Models of Slope Deposits of Combination Prograding/Aggrading Margins.....	17
Observations	17
Interpretation.....	18
Synthesis	19
Discussion.....	20
Challenges in Seismic Stratigraphic Interpretations	21
Application to Real-World Data	24
Geological Background	24
Loss of Geological Detail in Seismic Data	26
Interpreting Platform FX.....	27
Conclusions.....	31
References.....	33
Tables.....	64
Appendix 1: Illustrative Model Detailed Description.....	68

Introduction

Shelf margins throughout the geologic record document the history of ancient rift basins, passive margins, and other, more complex tectonic settings (Rich, 1951; Peyton, 1977; Van Wagoner et al., 1988; Sonnenfeld and Cross, 1993; Buchbinder and Zilberman, 1996; Kenter et al., 2001; Hanebuth and Stattegger, 2004). One special class of shelf margins, those that flank carbonate shelves and isolated platforms, include architecture and facies that are the products of numerous variables including tectonism, relative changes in sea level, climate, and hydrodynamic conditions (Epting, 1980; Eberli and Ginsburg, 1989; Bosence et al., 1998; Zampetti et al., 2004; Vahrenkamp et al., 2004; Van Vliet and Krebs, 2009; Betzler et al., 2013; Kosa et al., 2015). These variables and their interactions produce the complex geometries and facies patterns common on carbonate shelf margins (Grammer and Ginsburg, 1992; Lafranchi et al., 2011; Roesleff-Soerensen et al., 2012; Reolid et al., 2014).

Carbonate slope deposits, strata that occur on the flanks of shallow-water carbonate margins and dip towards the basin, represent part of carbonate shelf-associated sediment. Most slopes consist of sediment that is produced on the margin top and transported into deeper water, although they can include internal complexity as a result of depositional, erosional, and bypass dynamics (Schlager and Camber, 1986; Grammer et al., 1991; Rendle-Bühning and Reijmer, 2005; Warrlich et al., 2005; cf. Collins et al., 2013). Varied processes active on carbonate slopes, coupled with the first-order variables influencing margins, result in a wide range of depositional characteristics, including their relief, thickness, gradient, and geometric relationship with basinal strata.

Although parts of many carbonate margins and their slopes are exposed in outcrop (Achauer, 1969; Rudolph et al., 1989; Schlager et al., 1991; Sonnenfeld and Cross, 1993; Kenter

et al., 2001; Janson et al., 2007; Lafranchi et al., 2011; Ali, 2014; Reolid et al., 2014), an entire platform-slope-basin transect is not always preserved in the rock record in surface exposures. In contrast, seismic data provide unique, synoptic perspectives on carbonate margins and their evolution. Due to limited resolution of seismic data relative to the scale of stratigraphic heterogeneity, however, many features of carbonate margins may not be portrayed accurately in seismic data, and some data can be misinterpreted as an unconformity, when they are a pseudo-unconformity. Pseudo-unconformities (Rudolph et al., 1989) are reflectors which appear to be depositional unconformities based on reflector termination patterns (Mitchum et al. 1977), but instead are caused by rapid lateral changes in dip or facies (Stafleu and Schlager, 1995) and thus do not meet the sequence stratigraphic criteria for unconformities (Mitchum et al., 1977; Schlager et al., 1991). Pseudo-unconformities cut across timelines and complicate accurate interpretation of slope deposits and the architecture of carbonate margins (ibid.).

Seismic modeling provides a means to understand how architecture and petrophysical variability of carbonate margins might affect their seismic character (Rudolph et al., 1989; Stafleu and Schlager, 1991; Stafleu et al., 1993; Bracco-Gartner and Schlager, 1999; Kenter et al., 2001; Janson et al., 2007). These studies collectively have illustrated the efficacy of applying seismic modeling to individual real-world outcrops to improve understanding of subsurface seismic data. What remains missing is systematic analysis of how a variable repeatedly discussed in those studies, stratal architecture (i.e. distribution of petrophysically distinct facies within aggrading, prograding, and combination prograding and aggrading geometries), influences the seismic response of carbonate shelf margins. Synthetic seismic models produced in such a study, constrained by real-world seismic, outcrop, and well data, are applicable to many carbonate margin systems across time and space.

In this context, the objective of this study is to illuminate how changes in geology, even at thicknesses below seismic resolution, can impact seismic data characteristics such as amplitude, period, and reflector geometry and terminations. To achieve this end, this study utilizes a suite of seismic models designed to test a range of scenarios of idealized endmember geometries (prograding, aggrading, and combination prograding and aggrading carbonate shelf margins). Inspired and constrained by outcrop facies characteristics, seismic geometries, and well-log petrophysical data, this study explores how variations in facies-controlled petrophysical properties could produce changes in the seismic character of carbonate shelf margins.

Carbonate margin and slope geometries are sensitive indicators of paleobathymetry, hydrodynamics, sediment production and redistribution, and relative changes in sea level (see references above). Because of this, their accurate interpretation is crucial for understanding the nature and controls on spatio-temporal margin evolution (Sarg, 1988; Handford and Loucks, 1993; Bachtel et al., 2004; Kosa et al., 2015; Rankey, 2017; Rankey et al., 2019; Makhankova et al., 2020). Second, many carbonate systems serve as prolific hydrocarbon reservoirs (e.g. Miocene Central Luconia Province, Malaysia- Fui, 1978, Epting, 1980, Zampetti et al., 2003, 2004, Kosa et al., 2015; Tengiz Field, Kazakhstan- Collins et al., 2013; Natuna Platform- Rudolph and Lehman, 1989, Bachtel et al., 2004; Indonesia- May and Eyles, 1985; Permian Basin, West Texas- Galley, 1951; Ward et al., 1986). In these reservoirs, the nature of the relationship between margin and slope deposits can impact hydrocarbon production. In Central Luconia, for example, thief zones occur in association with low-relief margins where coarse-grained deltaic siliciclastics onlap the carbonate platform and siphon hydrocarbons out of the reservoir (Kosa et al., 2015). Alternatively, if they are not connected to the main reservoirs, slope deposits themselves can be secondary exploration targets in a region with a proven hydrocarbon system.

Background

A range of first-order variables influence the character of slope deposits, including margin architecture, slope sedimentology, and diagenesis. These factors in turn are products of biota and biotic evolution, structural evolution, hydrodynamic conditions, relative changes in sea level, and climate (Epting, 1980; Eberli and Ginsburg, 1989; Bosence et al., 1998; Vahrenkamp et al., 2004), as well as the timing and nature of the migration of meteoric, marine, and burial fluids through slope deposits. As such, it is impossible to model every conceivable geological scenario. This study focuses on the importance of stratal architecture to the seismic expression of carbonate margin and slope systems. It analyzes how facies distribution and stratal architecture control the seismic response of three endmember carbonate margin geometries. The effort does not consider post-depositional variables that influences character such as structural deformation (Zampetti et al., 2003, 2004; Vahrenkamp et al., 2004; Rankey et al., 2019; Makhankova et al., 2020) or fluid effects (Christiansen, 2009, Warrlich et al., 2010). Likewise, it does not explicitly model the impact of diagenesis on seismic expression (Neuhaus et al., 2004; Fournier and Borgomano, 2007; Warrlich et al., 2010; Teilet et al., 2020a), although its influences might be considered implicit in the petrophysical variability.

Physical Model Design

Each model consists of four parts: 1) a geological facies model constructed in the depth domain (example shown in Figure 1A; Table 1); 2) a reflectivity facies model, using facies-based P-wave velocities (V_P) and density (Figure 1B); 3) the same geological model, but converted to the time domain based on V_P (Figure 1C); and 4) a synthetic seismic model resulting from convolving a reflectivity facies model with a wavelet (Figure 1D).

At the largest scale, the models include three endmember shelf-margin geometries: aggradational, progradational, and combination aggradational/progradational. This study does not model or consider backstepping geometries, because slopes are typically not volumetrically significant since the excess sediment production required to accumulate thick slope deposits does not occur as a carbonate margin backsteps (Epting, 1980; Schlager et al., 1994). Petrophysical properties and large-scale architecture of the carbonate margin remain constant within each suite of models. For example, each of the ‘Slope Deposits of an Aggrading Carbonate Margin’ models (apart from the ‘Low-Relief Interfingering’ scenario) have the same general architecture and only slope petrophysical properties are varied.

General inspiration for the three endmembers comes from seismic data, primarily from Central Luconia Province (Malaysia) and the Browse Basin (Northwest Shelf, Australia), but designs of the variant models are constrained by outcrop and seismic data of other carbonate margins. These additional outcrops, described in a range of literature sources (Tables 2, 3, and 4), provide key geometries that are explored in this study.

Each of the eleven geological models used to generate seismic models for this study belongs to one of three of the previously mentioned endmember geometries: Aggradational, Progradational, and Combination Progradational and Aggradational. Every endmember consists of a suite of geological models, including one base model and one or more variant models. Each variant model adds an additional layer of complexity to its’ respective base model. Descriptions of each base geological model, their variant models, and variables tested through seismic modeling are as follows:

The suite of aggrading carbonate margin models (Figures 2 and 3, Table 2) test the impact of geometry and petrophysical variability on the seismic character of slope deposits. Each

geological scenario (Figures 2A, 2B, 3A, and 3B) maintains a consistent shelf evolution, with a uniform, laterally continuous layer of carbonate mud overlain by a basinward-thinning high-impedance carbonate unit. Atop this layer of high-impedance carbonate is the first phase of shelf growth consisting of thick platform and reef strata that thin towards the basin. These strata are capped by a sequence boundary, and in turn overlain by another layer of high-impedance carbonate. A second phase of shelf aggradation includes marked slope deposition; changes in its position, geometry, and thickness are the focus of this suite. These strata also are capped by a sequence boundary, which in turn is overlain by a thin bed of high-impedance carbonate and low-impedance basinal siliciclastics.

The Base scenario (Figure 2A) for the aggradational suite includes a single slope body with a maximum thickness of 40 meters (approximately the resolution of the 22 Hz wavelet). The three subsequent scenarios are variants of that base model, changing elevation of slope deposits relative to the margin top (High-Relief Bypass, Figure 2B), adding petrophysical variability within the slope body (Three-Layer Onlapping, Figure 3A), or adding offlapping slope geometries (3 Layer Offlapping, Figure 3B).

The Low-Relief, Interfingering scenario (Figure 4) also includes an aggrading margin but modifies architecture to model a scenario of interfingering between two intervals of carbonate slope deposits and basinal siliciclastics at thicknesses below the seismic resolution of a 22 Hz wavelet. Motivation behind this scenario comes from observations and interpretations of seismic data from Central Luconia and results from forward stratigraphic models constrained using data from Central Luconia (Kosa et al., 2015; Granjeon, 2020). Whereas the marked differences in margin architecture make direct comparison between this model and the other aggrading margin

models strained, observations at the margin and in the basin yield insights into how complex relationships in low-relief shelf-to-basin systems can influence seismic character.

The suite of prograding margin models evaluates the seismic character of prograding shelf margins, along with some changes in petrophysical properties in the reef and slope facies. Four models make up the prograding shelf suite: the Base model, Toe of Slope Lowstand model, the Flooding Interval model, and the Tight Clinoform model (Table 3). The Base scenario (Figure 5A) models a carbonate margin of several prograding sequences, each bounded by a sequence boundary. Within clinoforms, the slope deposits increase in acoustic impedance basinward in the Base model. All three variant models (Figures 7B, 8A, and 8B) utilize geometries similar to the Base model but include a change in geometry or absolute values of petrophysical properties. For example, the Toe of Slope Lowstand scenario (Figure 5B) includes a cemented, high-impedance interval in a portion of the reef with an associated low-impedance lowstand at the toe of slope. A second variant, the Flooding Interval scenario (Figure 6A), contains two reef intervals, one of high impedance and one of low impedance, and thin, high-impedance layers (i.e., muddy flooding intervals; cf. Reolid et al., 2014; Van Tuyl et al., 2018) that onlap slope deposits. A third variant is the Tight Clinoform scenario (Figure 6B), which incorporates an entire clinoform of high-impedance carbonate.

A third suite of models (Figure 7) explores the seismic expression of a prograding and aggrading shelf margin. Both models utilize the same stratigraphic architecture (Figure 7A, B), namely, clinoforms containing several sequence boundaries that gradually increase in gradient and relief and capped by low-impedance basinal siliciclastics. The model petrophysics vary, however. The first model (Figure 7A), referred to as the High Impedance Interior (HIMI) model, assigns a shelf interior V_P of 4700 m/s. In contrast, the second model, referred to as the Low-Impedance

Interior (LIMI) model (Figure 10B) simulates more porous shelf interior strata with a V_P of 3250 m/s.

Petrophysical Properties and Seismic Modeling

Within these geometries, impedance is controlled by facies. To reduce model complexity and isolate variables, this study uses facies-based impedance to model spatial changes in impedance (e.g., following Rudolph et al., 1989; Schlager et al., 1991; Janson et al., 2007). Facies-based modeling wherein each petrophysical facies (Table 1) represents specific geological facies (associated with a depositional environment) ensures geological realism in all the models. Studies of core and outcrop data demonstrate that V_P values in carbonate rocks do not directly correlate to one single variable such as burial depth, grain size, or mineralogy, but the best correlation exists between V_P values and porosity (Anselmetti and Eberli, 1993). As a result, an assumed porosity for each facies constrains the assigned V_P value. Each facies except for slope and reef facies is assigned one constant V_P and density (Table 2). Density for each facies are estimated from well data (Rankey et al., 2019), whereas V_P values are assigned based on core, well-log and outcrop data from literature (Anselmetti and Eberli, 1993; Anselmetti et al., 1997; Bracco-Gartner et al., 2002; Ali, 2014; Rankey et al., 2019). To further improve realism in models, acoustic impedance of slope facies is modeled to increase basinward, reflecting higher velocities related to grain size decrease and mud abundance increase with greater distance from the carbonate margin (Lafranchi et al., 2011; Reolid et al., 2014).

The reflectivity facies model was convolved (Peterson et al., 1955) with a zero-phase SEG-normal polarity Ricker wavelet (Ricker, 1953). The modeling software, RokDoc (Rittenhouse et al., 2017; Ferdinando et al., 2019), does not consider the interface between the lowermost facies

and the void space (base of the model) as an impedance interface, eliminating edge effects on the seismic character. Three frequencies (22, 60, and 75 Hz) included a 2 ms sampling rate and span the frequencies of seismic data available for comparison with results of this study (30 and 60 Hz), and an additional, best-case frequency further pushes model resolution (75 Hz).

The end products include three seismic models for each geological scenario. Considering a velocity of 4000 m/s, 22, 60, and 75 Hz wavelets have vertical seismic resolutions of approximately 45 m, 20 m, and 15 m, respectively. Although geometries modeled at or below the limit of seismic resolution are subject to display pseudo-unconformities (Rudolph et al., 1989; Stafleau and Schlager, 1991) and tuning effects (Widess, 1973), they provide insight by illustrating what characteristics (thickness, geometry, acoustic impedance values) most markedly influence seismic character.

Results- Seismic Models

In each suite of seismic models, reflectors of low-frequency (22 Hz) seismic models are numbered sequentially, from bottom to top, and described from left to right (shelf to margin to basin). The seismic models are described in terms of seismic character, defined by reflector amplitude, geometry, and termination patterns (Mitchum et al., 1977; Ramsayer, 1979; Bachtel et al., 2004). Low-frequency seismic models are the focus of this section, and higher-frequency models are discussed later. For detailed descriptions of every scenario, see Appendix I.

Models of Slope Deposits of an Aggrading Carbonate Shelf

Observations

Shelfward of the margin, each of the four seismic models in the aggrading suite consists of six reflectors, with three peaks (blue, reflectors 1, 3, and 5) and three troughs (red, reflectors 2, 4, and 6). Reflectors are continuous across the width of the model except reflector 4, which terminates at the margin as reflector 3 combines with reflector 5 (referred to as reflector 3/5). The shelfal portions (left of the reflector numbers) include parallel, horizontal, and continuous, moderate- to high-amplitude reflectors that dip basinward at the shelf margin. Because the focus of this study is on the seismic character of slope deposits, the focus of descriptions and comparison among models focus on seismic character in those areas, e.g., from the blue arrow to the basinward edge of each seismic model.

Comparing the Base model (Figure 2A) to the High-Relief Bypass model (Figure 2B) demonstrates the impact of synoptic shelf margin-basin relief on the seismic expression of a shelf margin. In both the Base and High-Relief Bypass models, the seismic character of reflector 3/5 changes where slope deposits onlap the margin (the blue arrows, Figures 2C, 2D). In both models, amplitude and period in reflectors 2 and 3/5 gradually decrease basinward. In the Base model, geometry abruptly changes with an increase in amplitude and decrease in dip angle of reflector 3/5. Reflectors 2 and 3/5 of the Base model also decrease in dip angle, but in the High-Relief Bypass model, amplitude decreases at the blue arrow. Additionally, around the blue arrow in the Base model, reflectors 2 and 3/5 undulate slightly for several traces but are even in the basin. By contrast, no comparable change is evident near the blue arrow in the High-Relief Bypass model.

Comparison among the Base model, the Three Layer Onlapping (Figure 3C), and Three Layer Offlapping (Figure 3D) seismic models tests the influence of petrophysical variability within a slope body and more complex stratal relationships between slope bodies on seismic character. Reflectors 2 and 3/5 in both the Base and Three Layer Onlapping models appear almost undulatory at the blue arrow. The primary difference between the Base and Three Layer Onlapping models is subtle, notably a more pronounced decrease in amplitude of reflector 2 of the Three Layer model compared to reflector 2 of the Base model. In the Three Layer Offlapping model, the amplitude decrease of reflectors 2 and 3/5 at the point of onlap is more pronounced than that of the Base model or the Three Layer Onlapping model. Additionally, reflectors 2 and 3/5 of the Three Layer Offlapping model are more concave than the Base and Three Layer Onlapping models.

Interpretation

Comparison among the suite of aggrading margin slope models tested the impact of two variables on the seismic character of slope deposits: 1) slope geometry (i.e. onlapping or offlapping, high or low shelf-to-basin relief), and 2) petrophysical variability within a single slope body. The results (Figure 8) reveal how subtle changes in reflector character suggest lateral changes in facies, even in data near seismic resolution.

For example, a change in reflector character (i.e., geometry and amplitude) between the Base (Figure 2C) and High-Relief Bypass (Figure 2D) models corresponds to the position where slope deposits onlap the margin. The differing amplitude and geometries of reflectors 2 and 3/5 at the blue arrow (cf. Figure 2C, 2D, 3C, & 3D) illustrate how the details of their seismic character varies with the acoustic impedance contrast between deposits of the slope and those of the shelf margin reef.

Similarly, contrasts among the Base (Figure 2C) and Three Layer Onlapping (Figure 3C) models illustrate how three stacked, petrophysically distinct layers within a single slope body result in subtle differences in seismic character. Both the Base (Figure 2C) and Three Layer Onlapping (Figure 3C) models showed changes in geometry and amplitude at the blue arrow in reflectors 2 and 3/5. Although there were additional differences in the amplitude and geometry at the blue arrows, those differences are too subtle to differentiate confidently between scenarios.

Collectively, these models also demonstrate how timelines such as sequence boundaries from the geological models (solid and dashed black lines in Figures 2A, 2B, 3A, and 3B) may, or may not, follow reflectors in the seismic models. These four models of aggrading shelves (Figures 2E, 2F, 3E, and 3F) map the lower sequence boundary (solid black line, left) as a trough on the shelf (reflector 2). The lower sequence boundary follows reflector 2 past the blue arrow, into the basin, where it deviates into the underlying peak (reflector 1), which marks that sequence boundary across the remainder of the model. The upper sequence boundary (dashed black line) lies near the zero-crossing of reflectors 4 and 5 to the shelf margin, where reflector 5 coalesces with reflector 3. There, the sequence boundary continues to follow reflector 3/5 past the blue arrow. Further basinward, the sequence boundary deviates from reflector 3/5 and drops to the zero-crossing between reflectors 2 and 3/5. Thus, the position of time lines, here the sequence boundaries, can vary considerably from amplitude maxima or minima, to zero-crossings.

Models of Slope Deposits of Low-Relief, Interfingering Shelf and Basinal Strata

Observations

Compared to the Base model (Figure 2C), reflectors 4, 5, and 6 of the Low-Relief Interfingering model (Figure 4B) all have markedly less relief and lower dip angles from the margin basinward. Additionally, all six reflectors in the slope-to-basinal portion of the Low-Relief Interfingering seismic model are chaotic to discontinuous, with additional, unnumbered reflectors in the basin.

Interpretation

Low shelf-basin relief, captured in the Low-Relief Interfingering model, appears to result in ambiguity in the lateral extent of reef and slope deposits (Figure 6). Subtle changes in geometry and amplitude mark the reef-slope transition in the Low-Relief Interfingering model, precluding confident interpretation. Comparing this model (Figure 4B) to the Base model (Figure 2C) illustrates how more complicated slope-basinal relationships might affect seismic character. In the 22 Hz seismic model (Figure 4B), a slight change from horizontal to basinward-dipping reflectors and decreased amplitude might suggest a facies transition, but the relatively simple nature of the reflectors (horizontal, parallel, and mostly continuous) belies the underlying geological complexity.

Overlaying the three time lines (sequence boundaries) from the geological model of the Low-Relief Interfingering model on the seismic data (Figure 4C) further illustrates how and why reflectors may, or may not, coincide with sequence boundaries. The lowest sequence boundary (solid black line) follows reflector 2 from the shelf to the shelf margin, crossing the interval where

reflector amplitude, geometry, and continuity vary considerably, and then continues in the zero-crossing between reflectors 2 and 3 in the basin. The middle sequence boundary (dashed line) follows the reflector 4 - reflector 5 positive-to-negative zero-crossing within the shelf, before switching to a negative-to-positive zero-crossing in the basin. Finally, the uppermost sequence boundary (upper solid black line) follows reflector 5 from the shelf to the shelf margin, where it deviates into the zero-crossing between reflector 5 and two different unnumbered reflectors further basinward.

Models of Slope Deposits of Prograding Carbonate Margins

Observations

The four seismic models in the prograding suite illustrate both similarities and differences. For example, in the low-frequency data, the Base (Figure 5A and 5C), Toe of Slope Lowstand (Figure 5B and 5D), and Flooding Intervals (Figure 6A and 6C) scenarios include four reflectors, whereas the Tight Clinoform (Figure 6B and 6D) scenario consists of six reflectors. With respect to geometry and continuity, seismic character in the models with four reflectors is consistent, in that reflectors are continuous across the width of the model, and dip basinward towards the edge of the model. Nonetheless, reflector amplitudes and period vary considerably among models. In those four models, reflector 1 is a moderate amplitude, horizontal peak parallel to the other reflectors and pinches out before reaching the edge of the model. Reflector 2 is a roughly horizontal trough parallel to other reflectors, it dips basinward before continuing to the edge of the model. Reflector 3 dominantly is a horizontal peak parallel to reflectors 2 and 4. It dips basinward at the same position as reflector 2, where it increases in amplitude towards the edge of the model.

The Flooding Interval model (Figure 6C) includes a subtle dip approximately two-thirds of the way across the model, before returning to a similar position. Reflector 4 is the upper, horizontal trough at the top of the model. It runs parallel to reflector 3 and continues to the model edge.

The primary differences among the four models are variations in reflector amplitude relative to the Base model. For example, reflector 2 of the Toe of Slope Lowstand model (Figure 5D) includes two amplitude bursts elevated relative to the amplitudes in the middle of the model, to the left of the yellow arrow. Additionally, the doublet of reflector 2 in the leftmost portion of the Toe of Slope Lowstand scenario (Figure 5D) is lower in amplitude than in the Base model (Figure 5C).

Like in the Toe of Slope Lowstand model, reflectors 1, 2, and 3 of the Flooding Interval model (Figure 6C) differ from the Base model in amplitude, period, geometry, and lateral extent. Specifically, reflector 1 is lower amplitude and less laterally extensive in the Flooding Interval model than reflector 1 of the Base model. Reflector 2 has a doublet trough like the Base model, but this doublet occurs further basinward in the reflector, and persists across two-thirds of the model. Additionally, reflectors 2 and 3 both include a high-amplitude trough and peak, respectively, to the left, but decrease to moderate amplitude approximately one-third of the way across the model. The final difference is the divot in reflector 3 near the middle of the model.

The reflectors of the Tight Clinoform model (Figure 6D) also are distinct from those of the Base seismic model. Reflector 1 is a moderate-amplitude trough that is truncated the edge of the model. Reflectors 2 and 3 form a high-amplitude trough and peak pair that dip gently basinward. Approximately one-third across the model (yellow arrow in Figure 6D), both reflectors increase in dip angle and decrease in amplitude. Reflectors 4 and 5 form parallel, moderate-amplitude, horizontal to subtly basinward dipping, trough-peak pair that onlap reflector 3. The top reflector,

reflector 6, is a moderate-amplitude, horizontal trough which runs across the top of the model, parallel first to reflector 3 and then reflector 5. Reflector 6 dips basinward and increases in amplitude at the same position as reflectors 4 and 5 and continues to the edge of the model.

In models of higher frequency (Figures 5G, 5H, 5G, and 5H), the number and complexity of reflectors within the slope deposits increases. These additional reflectors more accurately depict the progradation of the margin in each of the four models.

Interpretations

These results reiterate how changes in reflector character can suggest changes in facies or petrophysical properties (Figure 10). Two of the low-frequency models (Toe of Slope Lowstand - Figure 5D, and the Flooding Interval - Figure 6C) include lateral changes in reflector amplitude and geometry that correspond to changes in petrophysical properties within the reef or slope facies. The amplitude burst in reflectors 1 and 2 of the Toe of Slope Lowstand model (Figure 5D) are related to the low-impedance interval at the toe of slope, and the amplitude burst in reflectors 2 and 3 of both the Toe of Slope Lowstand and the Flooding Interval models correspond to the high-impedance interval in the reef facies.

Some similarities between the Flooding Interval model and the Tight Clinoform model reveal how different geological scenarios (e.g. a low-impedance zone in the reef or an entire high-impedance clinoform) can produce similar seismic responses. In the Flooding Interval model (Figure 6C), the portions of reflectors 2 and 3 basinward of the yellow arrow could be interpreted onlapping more shelfward portions of those reflectors and marking a sequence boundary at the position of the yellow arrow. This interpretation resembles reflector terminations in the Tight

Clinoform model (Figure 6D), wherein reflectors 4 and 5 onlap reflector 3 at the yellow arrow, indicative of a seismic sequence boundary.

The 22 Hz models for this suite of scenarios illustrate how geological information applicable to seismic stratigraphic interpretation is subtle in units below seismic resolution. Similarly, many of the low-frequency models only have one sequence boundary that can be defined using reflector terminations (Mitchum et al. 1977); this surface is the top of carbonate, which might be recognized by toplap or onlap (Figure 6C, D). Higher-frequency models (Figures 5G, 5H, 6G, and 6H) more accurately capture seismic geometries, showing both the offlapping reflectors within the shelf, and clearly imaging the top-carbonate reflector.

Models of Slope Deposits of Combination Prograding/Aggrading Margins

Observations

Seismic character varies markedly between the low-frequency seismic models of the two scenarios in this suite. The low-frequency HIMI model (Figure 7C) consists of four reflectors. Reflector 1 is a moderate-amplitude, sub-horizontal peak which terminates against reflector 2 towards the basin. Reflector 2 is a moderate-amplitude, horizontal, and continuous trough. It shows a basinward decrease in amplitude and period at the shelf break. Reflector 3 is a high-amplitude, horizontal peak, with a subtle basinward decrease of amplitude. At the shelf margin, the reflector dips basinward steeply and period decreases. Amplitude and period increase basinward and the reflector returns to horizontal before reaching the edge of the model. Reflector 4 is a moderate-amplitude, horizontal trough which runs parallel to reflector 3. It dips basinward at the same point as reflector 3 and increases in amplitude and period before reaching the edge of the model.

Seismic character of the low-frequency LIMI (Figure 7D) model is more complex than that of the HIMI and includes more numerous and more complex reflectors. The LIMI model consists of six reflectors, three peaks and three troughs. Reflector 1 is a moderate-amplitude, shelfward-dipping reflector which runs parallel to reflector 2. Reflector 2 is a moderate-amplitude, shelfward-dipping trough parallel to reflectors 1 and 3. The reflector dips basinward at the shelf margin and decreases in period before disappearing at the bottom of the model. Reflector 3 is a moderate-amplitude, convex-upward peak roughly parallel to reflector 2. Amplitude increases near the high point, where the reflector dips reverse, and decrease in period. Amplitude and period both increase basinward as the reflector flattens and reaches the edge of the model. Reflector 4 is a moderate-amplitude, shelfward-dipping trough which appears to onlap reflector 3 behind its high point. Reflector 5 is a low-amplitude and horizontal peak that also appears to onlap reflector 3. Reflector 6 is a low-amplitude, horizontal trough which increases in amplitude moving to the right. Its dip angle increases at the same position as reflectors 2 and 3, increasing in amplitude and period, before flattening and reaching the edge of the model.

Models of higher frequency (Figures 7G and 7H) again show an increase in the number and complexity of reflectors within the slope deposits. These additional reflectors more thoroughly capture the geometry of the margin.

Interpretation

Comparing the HIMI and LIMI models (Figure 11) demonstrates the marked impact that the petrophysical properties can have on the seismic expression and interpretation of a carbonate margin. The LIMI model demonstrates how a high impedance contrast between shelf interior and

reef facies might produce a pseudo-unconformity, wherein a reflector (reflector 3 in Figure 7D) follows a facies boundary across time lines (the solid lines in Figure 7F).

Overlaying the time lines from geological models on corresponding 22 Hz seismic models (Figure 7E and 7F) reiterates that both the low-frequency models misrepresent the number or nature of potential seismic stratigraphic time lines. In the 22 Hz HIMI model (Figure 7E), only the uppermost surface, the top-carbonate surface (reflector 3 in Figure 7C), forms a single reflector across the whole model. In the 60 Hz HIMI model (Figure 7G), seismic stratal surfaces within the slope are distinct and discernable. The 22 Hz LIMI model (Figure 7F) is distinct. It images only the top carbonate sequence boundary, but even so, it does so only for the portion of the model to the right of where reflectors 4 and 5 appear to onlap reflector 3 (yellow arrow in Figure 7F). Additionally, the onlap of shelf interior reflectors 4 and 5 onto reflector 3 in the 22 Hz LIMI, 60 Hz LIMI, and 60 Hz HIMI (Figures 7F, 7H, and 7G, respectively) could be interpreted as to represent seismic sequence boundary.

Synthesis

These simple models demonstrate the seismic response to known geology. Collectively, they illustrate a range of scenarios of the expression of carbonate shelf margins in seismic data at several frequencies. Comparison among model sets (Figures 8, 9, 10, and 11) reveals several themes. First, across every suite of models, changes in reflector character (amplitude, period, and geometry) suggest lateral changes in petrophysical properties or facies transitions (cf. Kenter et al., 2001; Teillet et al., 2020b). Second, in addition to demonstrating how petrophysical variability influences seismic character, results reveal that many time lines, such as sequence boundaries, deviate from a single reflector, particularly where there is a lateral change in facies or termination

of units (Eberli et al., 2002; Janson et al., 2007). Finally, the petrophysical properties (and thus the magnitude of acoustic impedance contrast) play a critical role in the seismic expression of a carbonate margin (Kenter et al., 2001; Eberli et al., 2002; Janson et al., 2007).

As useful as the results and insights may be, they do include limitations. Relying on changes in seismic character (amplitude, period, or geometry) becomes difficult in low-relief situations, particularly where there are complex relationships between carbonate and basinal siliciclastics (e.g., Figure 4). Without high impedance contrasts among the reef, slope, and basinal siliciclastic facies, much of the stratigraphic detail can be hidden. In such a situation, no marked changes in reflector geometry would mark a change in facies. These challenges are not limited to low-frequency data, as even the 60 Hz model for the Low-Relief Interfingering scenario (Figure 4D) only subtly improved definition of facies transitions, or the base and top of slope deposits.

Discussion

Seismic data serve as an invaluable tool by which to evaluate the complex geometries and geology of carbonate isolated platforms and rimmed shelves (Eberli and Ginsburg, 1989; Masaferrro et al., 2004; Kosa et al., 2015). Unfortunately, the ambiguity inherent in seismic data, especially at low frequencies, presents a challenge to accurate understanding of the complexity of carbonate margins (Schlager et al., 1991; Stafleau and Schlager, 1995; Janson et al., 2007). These challenges are magnified at shelf margins, where marked gradients, complex rapid lateral facies changes and interfingering among shelf, slope, and basinal strata occur (Kosa et al., 2015).

Challenges in Seismic Stratigraphic Interpretations

The non-unique nature of seismic data, coupled with low resolution relative to the scale of geological complexity, favors conditions that enhance the possibility of incorrect seismic stratigraphic interpretations. Several scenarios demonstrate plausible, but incorrect, seismic stratigraphic interpretations and how these errors might be avoided by considering the possible underlying geological complexity.

One example of possible misinterpretation comes from the progradational shelf margin suite of models. The 22 Hz Prograding Margin with Flooding Intervals model (B) could be incorrectly interpreted in several ways (marked by the dashed lines in Figure 12A-C), especially in the absence of well data and a constrained conceptual model. The first interpretation (Figure 12A) has mounded geometries basinward, with karst or an erosional channel in the divot of the upper two reflectors, and a high-impedance layer overlying low-impedance, low-relief clinoforms. A second, alternative interpretation might suggest low-impedance tops of low-relief clinoforms onlapped by a more basinward shelf margin and overlain by a hard flooding interval (Figure 12B). A third interpretation (Figure 12C) could include low-impedance clinoforms overlain by a high-impedance flooding interval. The main difference between this interpretation and the previous is the number and geometry of clinoforms within the prograding margin.

All three of these interpretations are incorrect in several ways. For example, they misinterpret the cause of the uppermost peak as a single high-impedance layer overlying the clinoforms within the system instead of the reef top of a prograding system. Without well data or an accurate conceptual model, this mistake could push the interpretation of the top of the seismic unit to the peak (blue). Yet, the divot (yellow arrow in figure 8C) might be interpreted incorrectly

as an erosional channel or karst when it is caused by a low-impedance interval within the reef facies.

The correct interpretation (Figure 12D) demonstrates the complexity within the prograding margin model and emphasizes loss of critical detail if the geological complexity is below the limits of seismic resolution. What is revealed to be a series of clinoforms in higher-frequency data (Figure 12E) is reduced in the 22 Hz data to four dominantly horizontal, parallel reflectors with no marked indicators of the complex internal architecture, particularly within the slopes. These reflectors do show subtle changes in amplitude (e.g., the bursts to the far left of the model) and geometry (the divot near the margin and basinward dip of reflectors at the margin). Not surprisingly, more detail is evident in the 60 Hz seismic model (Figure 12E). In that model, basinward-dipping reflectors in the margin slope deposits coincide with high-impedance intervals onlapping clinoforms (muddy flooding surfaces, green lines, Figure 12F). Other internal reflectors within the margin slope deposits onlap or downlap onto the flooding surface reflectors.

A second example for potentially misinterpreting low-frequency seismic data is provided by the 22 Hz Low-Relief Interfingering seismic model (Figure 13A-E). The first incorrect interpretation (Figure 13A) posits mostly horizontal, parallel reflectors of an aggrading margin that is bounded by a steeply dipping surface (the bold, black dashed line). This margin in turn is onlapped by lower-amplitude, horizontal to undulating reflectors. These geometries could be interpreted to reflect basinal strata, with more complex geometries in the upper portions of the section. The sag in the onlapping strata, coupled with a low-amplitude, horizontal trough which onlaps both the margin and other basinal reflectors, suggests a second seismic sequence boundary marked by an erosional channel. Yet, the change in reflector character interpreted as onlap is the

result of the transition from margin to basin, where thinner high- and low-impedance intervals occur (Figure 13E).

A second potential misinterpretation (Figure 13B) could suggest sub-horizontal reflectors across the area, from shelf margin to basin. Like the previous interpretation, this incorrect interpretation has the low-amplitude trough onlapping the margin, and other basinal strata that define an erosional channel. The channel interpretation is the product of constructive interference between sidelobes of the two tongues of slope deposits (cf. Figure 13E). The resultant pseudo-onlap of the discontinuous, low-amplitude reflector onto a basinal reflector reflects slope tongues too thin to produce a detectable seismic response. Plotting timelines (the three sequence boundaries) from the input geological facies model onto the seismic data (Figure 13C) reveals that these timelines do not remain on one reflector; reiterating that seismic stratigraphic interpretation could be difficult if a timeline were simply carried on a trough or peak. Convolving the geological model with a 60 Hz wavelet (Figure 13D) adds more reflectors, but the complex geology of the system still is masked by the seismic character. Subtle increases in dip direction and intervals of lower amplitude suggest a change in facies, but the low shelf-to-basin relief and thin carbonate and shale bodies preclude an unambiguous correct interpretation.

A final example of misinterpretation incorporates the Low Impedance Interior Model. These data could be interpreted to include an asymmetric mounded geometry that is in turn onlapped by several sub-horizontal reflectors (arrowed dashed lines, Figure 14A). This apparent onlap would suggest that a ‘top-mound’ reflector is a seismic sequence boundary, delineating the top of a “pinnacle” carbonate platform (Kosa et al., 2015). Comparison with timelines (Figure 14B) demonstrates that the ‘top-mound’ reflector cross cuts stratal surfaces, and thus the apparent onlap surface represents pseudo-unconformity, created by an impedance contrast that cuts across

timelines. The interpretation represents the uppermost sequence boundary accurately, from the shelf margin into the basin, however. Convolving the model with a 60 Hz wavelet (Figure 14C) provides additional details in the form of offlapping reflectors within the slope deposits, geometries difficult to reconcile with a ‘mound’ interpretation.

Altogether these plausible, yet incorrect, interpretations of seismic data illustrate the potential pitfalls of interpreting seismic data without the benefit well log or core data to understand geology. They also emphasize how subtle changes in seismic character suggest important geological information such as facies boundaries and high- or low-porosity zones within a carbonate shelf system.

Application to Real-World Data

The final section of this study demonstrates application of the modeling to interpretation of real-world seismic data. A first example illustrates how geometric details, such as those evident in 60 Hz seismic data that formed some of the inspiration for the models herein, might appear in low-frequency (22 Hz) data. Subsequently, insights from seismic modeling provide guidance for interpreting seismic data of a real carbonate platform.

Geological Background

Seismic data utilized for this study come from two regions: 1) Central Luconia Province of the Sarawak Basin off the northwestern coast of Borneo, Malaysia, in the South China Sea, and 2) Browse Basin of the Northwest Shelf, Australia, Indian Ocean. Whereas both regions contain isolated carbonate platforms of middle Miocene age, they reflect different climate, sedimentologic, and tectonic history and, as a result, vary in geometry.

Central Luconia isolated carbonate platforms nucleated and grew atop extensional elevated fault blocks (Epting, 1980; Vahrenkamp et al., 2004; Ali, 2014). At the same time, intermittent uplift of Borneo produced siliciclastic sediments that were shed into the Sarawak Basin. These siliciclastics either interfinger with, or onlap, carbonate slope deposits, depending on the location of a platform relative to Borneo (Kosa et al., 2015). Platforms in Central Luconia include phases of aggrading, prograding and backstepping geometries, based on varying subsidence rates within the basin, eustatic change, and rate of siliciclastic influx (Epting, 1980; Bracco-Gartner et al., 2002; Vahrenkamp et al., 2004; Zampetti et al., 2004; Rankey et al., 2019). Some Central Luconia platforms are prolific hydrocarbon reservoirs, and many are made up of alternating high- and low-porosity (and impedance) layers within the platform interior (Vahrenkamp et al., 2004; Zampetti et al., 2004; Warrlich et al., 2010, 2019) which can result in multiple reservoir intervals in a single platform.

In comparison, Browse Basin platforms grew on a northwesterly dipping shelf. Non-tropical carbonate ramps in the Eocene through early Miocene transitioned to tropical rimmed shelves and isolated platforms in the middle Miocene, some lasting until the present (Struckmeyer et al., 1998; Roesleff-Soerensen et al., 2012; Belde et al., 2017). Platform geometries are dependent on variable subsidence rates, which varied across the basin. Platforms in the north of the basin include thick, aggrading geometries, whereas their counterparts to the south have dominantly progradational geometries (Belde et al., 2017).

This project uses seismic data from both the Browse Basin and Central Luconia. The Browse Basin seismic data have a central frequency of 60 Hz. Seismic data from Central Luconia have a central frequency of 30 Hz and includes Platform FX (Vahrenkamp, 1998; Warrlich et al., 2019; Makhankova et al., 2020).

Loss of Geological Detail in Seismic Data

Carbonate platform margins of parts of the Browse Basin are imaged by high-resolution seismic data with central frequency of 60 Hz. As such, they mimic the high-frequency seismic models and capture considerable variability in shelf margin and slope deposit geometries. The stratigraphic architectural details captured in the high-frequency data (Figure 15A, 15B, and 15C) provided some of the inspiration for the Aggrading Margin Slope, Prograding Margin, and Combination Prograding and Aggrading suites of models (Figures 15D-L). An interesting question is how these sorts of shelf-margin geometries would appear at lower frequencies, and what geological detail might be identifiable.

Results from this exercise reveal a marked decrease in the number and complexity of reflectors for each 60 Hz figure. The 22 Hz model for the Aggrading Margin Slope scenario (Figure 15J) reduces the seismic response of the slope deposits from four reflectors (bounded by the light blue and light green horizons in Figure 15A) to two, hiding the onlap of slope deposits onto the carbonate margin. Rather, only changes in reflector geometry and amplitude signal the transition from margin reef to slope deposits.

Likewise, the 22 Hz model of a prograding margin (Figure 15K) reduces the complex series of offlapping clinoforms and reflectors to more-or-less horizontal and parallel reflectors that are continuous across the model. Only the most shelfward part of the downlap surface (reflector 1 in Figure 5A) and top carbonate (reflector 3) are readily identifiable, and the clinoforms within the slope deposits are nonexistent.

Finally, the 22 Hz model of the prograding and aggrading shelf margin (Figure 15L) served as inspiration for Low-Impedance Interior model (Figure 15F). Much like the prograding margin, the 22 Hz model completely masks clinoforms of reef and slope deposits. Additionally, the margin

interior-reef facies boundary produces a pseudo-unconformity that could be interpreted incorrectly, as discussed earlier.

These reduced-frequency seismic figures illustrate how lower-frequency seismic data, like the data from Central Luconia, can hide important geological detail in seismic data. Several facies can have complex stratal relationships with one another in a relatively small package (3-5 reflectors) of reflectors. Rather than depending explicitly on reflector termination patterns to interpret seismic data, these results suggest interpretation could consider subtle changes in seismic character (i.e. a change in reflector geometry or amplitude) that might mark lateral changes in facies. Additionally, results from these models (Figures 2-10) indicate that seismic data are prone to masking sequence boundaries within seismic volumes.

Interpreting Platform FX

A final exercise demonstrates how seismic modeling might be applicable in interpretation of real-world seismic data. To that end, integrating seismic data from Platform FX (Figure 16A) with core description (Ali, 2014; Warrlich et al., 2019) provided the basis for seismic stratigraphic interpretation of Platform FX (Figure 16B). The seismic data, coupled with core descriptions, identify four major seismic stratigraphic surfaces within the platform that can be carried off platform. These core data (discussed by Ali, 2014 and Warrlich et al. 2019, not documented as part of this study) suggest that these surfaces represent flooding surfaces (blue and magenta solid lines, and black dashed line) and a coincident subaerial exposure and flooding surface (lime green solid line). All four surfaces present on the platform can be correlated to the basinal section using stratal terminations (Mitchum et al., 1977), with an additional surface of downlap (red solid line) limited to the basin.

These data illustrate several geometries akin to those from the models. One set is evident among the four major seismic stratigraphic surfaces near and basinward of the northwestern margin of Platform FX (Figure 16A-C). The other set, which is a smaller scale, includes only surface D (top carbonate) on Platform FX's southeastern margin (Figure 16A, 17). Surfaces B and C lie below the interval of interest on this southeastern margin.

The lowest mapped surface, surface A (blue solid line; Figure 16C), runs from platform to basin, where it is overlapped by basinal strata. On the platform, the second surface, surface B (lime green solid line), in core has been recognized as a subaerial exposure surface and a flooding surface. In seismic, surface B continues across the platform, but truncates reflectors at the platform margin. In the basin, overlying reflectors overlap it at the previous margin. A third surface, B', is defined present only in the basin, where it is overlapped. Thus, the package B-B' is present only in the basin. The fourth surface, surface C (magenta line), has been described in core as a flooding surface. At the platform margin, it appears to truncate older strata, and coincides with the top-carbonate reflector (surface D) in the slope and basin (e.g., basinward of the blue arrow in Figure 16B). At the yellow arrow, Surface C diverges from top carbonate, where it is overlapped and overlapped by other basinal strata. Surface D is the final surface, described in core as a flooding surface. It caps a succession present only on the platform top, where it represents the termination of carbonate production on Platform FX; this surface is overlain by shale.

Combining core data, the seismic stratigraphic geometries and surfaces, and insights from the modeling exercise yield a plausible interpretation of the facies of the northwestern margin of Platform FX (Figure 16C). In this area, each surface-bounded interval within the platform (e.g., A-B, B-C, etc.) corresponds to an interval of basinal slope deposits. The package of basinal reflectors between surfaces B and B' overlap onto surface B and are overlapped by overlying

reflectors. These reflector termination patterns, and the core data that illustrate that surface B is a coincident subaerial exposure surface and a flooding surface, imply that this slope body is a lowstand deposit, restricted to the basin. Surface A and the merged surfaces A-B are therefore sequence boundaries, overlain in the basin by lowstand strata of the seismic unit between B and B'.

The succession between the surface B' and top carbonate bounded by the yellow and blue arrows includes reflectors with geometry and amplitude trends analogous to the seismic models. For example, the package of three reflectors (two peaks and a trough) show an abrupt basinward increase in amplitude that corresponds with a basinward decrease in dip angle (Figure 16, the position denoted by the blue arrow). This abrupt change in amplitude and geometry at the blue arrow is similar to the changes in reflector character at the point of onlap in the Aggrading Margins suite of models (e.g., the blue arrow in Figure 2C). The blue arrow therefore is interpreted to mark the onlap of slope deposits onto the platform margin. This succession between surfaces B' and C in the basin are therefore interpreted as slope deposits of a highstand systems tract equivalent to platform top strata, with by onlap representing bypass of a steep margin (Playford, 1980; Schlager, 1989, 1991).

Further basinward, the interval bounded by surfaces C and D in the basin (left of the yellow arrow in 16B), also include reflector geometries analogous to those in a model. Here, a basinal reflector onlaps surface C; further basinward, this reflector downlaps onto surface C, and is in turn overlapped by another basinal reflector. These shingled, basinal geometries are similar to seismic geometries in the 60 Hz model of the Three Layer Offlapping scenario (Figure 3H), whose architecture are the result reflect offlap of several slope bodies. Based on these observations, the package of reflectors basinward of the yellow arrow and bounded by surfaces C and D at the base

and top, respectively, are interpreted as a package of highstand strata equivalent to the final phase of platform growth.

The southeastern margin includes another suite of geometries that may be informed by the modeling. Here, the final phase of growth on the platform, bounded by surfaces C and D (Figure 17), consists of a set of offlapping, basinward-dipping reflectors which downlap onto surface C. Each successive prograding reflector includes subtle aggradation, such that the succession appears to climb subtly in a series of stair steps. Two additional seismic lines (Figures 17C and 17E) lie approximately one kilometer to the southwest and two kilometers to the northeast, respectively, and show broadly analogous geometries.

Observations of reflector character coupled with insights from the modeling facilitate facies interpretations (Figures 17B, 17D, and 17E). Specifically, the shingled reflectors that climb in each clinoform resemble geometries in the 60 Hz LIM1 model (Figure 7G). These data thus are interpreted to collectively represent the downlap of highstand strata, final stage of platform growth. The subhorizontal portion of each shingled reflector is interpreted to be an interval platform interior, reef, and upper slope strata. The apparent subtle basinward climb of these reflectors suggest an aggradational component, and the trough that appears to climb represents the reef-platform interior contact (compare Figure 17A and 7G)

Therefore, observations of reflector character and termination patterns in conjunction with insights from modeling help constrain plausible interpretations of the margins of Platform FX, and support interpretations of how the platform evolved in space and time.

Conclusions

The geology and architecture of carbonate shelf margins are the result of a host of controlling factors, and seismic data can serve as a critical means of understanding and predicting their geological evolution and reservoir properties. To better understand how different geological scenarios might appear in seismic data, this study used a suite of seismic models to explore how varying the distribution and petrophysical properties of carbonate shelf strata within conceptual seismic geometries influences their seismic character.

Evaluating seismic character of the eleven seismic models enhanced understanding of how petrophysical variability within a shelf margin influences seismic character. Results from the modeling indicate the following:

1) Subtle changes in reflector character (amplitude, period, and geometry) can suggest lateral changes in facies or petrophysical properties.

In seismic data, geological detail can be below resolution. Even so, subtle changes in reflector character can suggest facies transitions or zones of petrophysical variability within individual facies. For example, models from the aggrading suite indicate that the reef-to-slope facies transition is characterized by an increase in dip angle and a decrease in reflector amplitude and period.

2) In addition to resolution issues, seismic data can obscure geometry of time lines such as sequence boundaries in carbonate shelf margins.

Seismic models from all three endmember geometries demonstrate how seismic data can complicate the interpretation of time lines and sequence boundaries. In the Aggrading Carbonate Margin suite, sequence boundaries deviate from reflectors where in areas with lateral facies changes (i.e., the lower sequence boundary in Figures 2E, 2F, 3E, and 3F) or

where the units terminate (i.e., the upper sequence boundary in Figures 2E, 2F, 3E, and 3F). The Prograding Carbonate Margin suite (Figures 7E, 7F, 8E, and 8F) demonstrated how seismic data might oversimplify the slope reflectors of a carbonate margin and under-represent the number of resolvable sequence boundaries. Finally, the LIM1 model of the Combination Prograding and Aggrading Carbonate Margin suite (Figure 10F) illustrates how the impedance contrast between the platform interior facies and reef deposits can produce a pseudo-unconformity and result in an inaccurate interpretation of a carbonate margin (Figure 14A).

3) Lessons from the modeling exercise, applied to real seismic data, constrain plausible seismic interpretation of an isolated carbonate shelf margin.

The final section illustrates how observations of seismic reflector amplitude, geometry, and location within a carbonate shelf system might be applied to seismic interpretation. Modeling results provided key insights for interpretations of platform architecture and facies distribution within Platform FX.

These results emphasize how seismic data may not fully capture the complexity of carbonate shelf margin systems, but that subtle changes in reflector character can be indicative of larger-scale geologic changes. Models such as these can constrain plausible interpretations of the facies distribution and architecture of carbonate shelf margins in seismic data.

References

- Achauer, C.W., 1969, Origin of Capitan Formation, Guadalupe Mountains, New Mexico and Texas: American Association of Petroleum Geologists Bulletin, v. 53, p. 2314-2323.
- Ali, M.Y., 2014, An integrated analysis of the depositional control, sedimentology and diagenesis of Cenozoic carbonates from the Sarawak Basin, East Malaysia: unpublished Ph.D. Dissertation, Imperial College, London, p. 1-467.
- Anselmetti, F.S., and Eberli, G.P., 1993, Controls on sonic velocity in carbonates: PAGEOPH, v. 141, p. 287-323.
- Anselmetti, F.S., and Eberli, G.P., 1997, Sonic velocity in carbonate sediments and rocks, *in* Palaz, I., and Marfurt, K.J., eds., Carbonate seismology: Society of Exploration Geophysicists Geophysical Development Series, v. 6, p. 53– 74.
- Anselmetti, F.S., Eberli, G.P., and Bernoulli, D., 1997, Seismic modeling of a carbonate platform margin (Montagna della Maiella, Italy): Variation in seismic facies and implication for sequence stratigraphy, *in* Palaz, I., and Marfurt, K.J., eds., Carbonate seismology: Society of Exploration Geophysicists Geophysical Development Series, v. 6, p. 373–406.
- Bachtel, S.L., Kissling, R.D., Martono, D., Rahardjanto, S.P., Dunn, P.A., and MacDonald, B.A., 2004, Seismic stratigraphic evolution of the Miocene-Pliocene Segitiga Platform, East Natuna Sea, Indonesia: the origin, growth, and demise of an isolated carbonate platform, *in* Eberli, G.P., Masferro, J.L., and Sarg, J.F., eds., Seismic imaging of carbonate reservoirs and systems: American Association of Petroleum Geologists Memoir 81, p. 309-328.

- Belde, J., Back, S., Bourget, J., and Reuning, L., 2017, Oligocene and Miocene carbonate platform development in the Browse Basin, Australian Northwest Shelf: *Journal of Sedimentary Research*, v. 87, p. 795–816.
- Betzler, C., Fürnstenau, J., Ludmann, T., Hubscher, C., Lindhorst, S., Paul, A., Reijmer, J.J.G., and Droxler, A.W., 2013, Sea-level and ocean-current control on carbonate-platform growth, Maldives, Indian Ocean: *Basin Research*, v. 25, p. 172-196.
- Bosence, D., Cross, N., and Hardy, S., 1998, Architecture and depositional sequences of Tertiary fault-block platforms; and analysis from outcrop (Miocene, Gulf of Suez) and computer modeling: *Marine and Petroleum Geology*, v. 15, p. 203-221.
- Bracco-Gartner, G.L., and Schlager, W., 1999, Discriminating between onlap and lithologic interfingering in seismic models of outcrops: *American Association of Petroleum Geologists Bulletin*, v. 83, p. 952– 971.
- Bracco-Gartner, G.L., Morsilli, M., Schlager, W., and Bosellini, A., 2002, Toe-of-slope of a Cretaceous carbonate platform in outcrop, seismic model and offshore seismic data (Apulia, Italy): *International Journal of Earth Sciences*, v. 91, p. 315-330.
- Buchbinder, B., and Zilberman, E., 1996, Sequence stratigraphy of Miocene-Pliocene carbonate-siliciclastic shelf deposits in the eastern Mediterranean margin (Israel): effects of eustasy and tectonics: *Sedimentary Geology*, v. 112, p. 7-32.
- Christiansen, C.L., 2009, Seismic attributes for carbonates: unpublished Master's Thesis, University of Bergen, p. 1-147.
- Collins, J., Narr, W., Harris, P.M., Playton, T., Jenkins, S., Tankersley, T., and Kenter, J.A.M., 2013, Lithofacies, depositional environments, burial diagenesis, and dynamic field behavior in a Carboniferous slope reservoir, Tengiz Field (Republic of Kazakhstan), and

- comparison with outcrop analogs, *in* Verwer, K., Playton, T.E., and Harris, P.M., eds., Deposits, architecture and controls of carbonate margin, slope and basinal settings: SEPM (Society of Sedimentary Geologists) Special Publication 105, p. 50-83.
- Eberli, G.P., and Ginsburg, R.N., 1989, Cenozoic progradation of Northwestern Great Bahama Bank, a record of lateral shelf growth and sea-level fluctuations: SEPM (Society of Sedimentary Geologists) Special Publication 44, p. 339-351.
- Eberli, G.P., Anselmetti, F.S., Kroon, D., Sato, T., and Wright, J.D., 2002, The chronostratigraphic significance of seismic reflections along the Bahamas Transect: *Marine Geology*, v. 2002, p. 1-17.
- Epting, M., 1980, Sedimentology of Miocene carbonate build-ups, Central Luconia, offshore Sarawak. *Geological Society of Malaysia Bulletin*, v. 12, p. 17-30.
- Ferdinando, D.D., Harrison, P.V., Stanbrook, D.A., 2019, Shooting for the stars: unravelling a Late Jurassic turbidite petroleum system- frontiers for the next generation of exploration: *West Australia Basin Symposium 2019 proceedings*, p. 1-19.
- Fournier, F., and Borgomano, J., 2007, Geological significance of seismic reflections and imaging of the reservoir architecture in the Malampaya gas field (Philippines): *American Association of Petroleum Geologists Bulletin*, v. 91, p. 235-258.
- Galley, J.E., 1958, Oil and geology in the Permian Basin of Texas and New Mexico, *in* Weeks, L.G., ed., *Habitat of oil*, American Association of Petroleum Geologists Special Publication 18, p. 395-446.
- Grammer, M.G., Ginsburg, R.N., and Harris, P.M., 1991, Timing of deposition and failure of steep carbonate slopes, Tongue of the Ocean, Bahamas: *American Association of Petroleum Geologists Bulletin*, v. 75, p. 107-131.

- Grammer, G.M., and Ginsburg, R.N., 1992, Highstand vs. lowstand deposition on carbonate platform margins: insight from Quaternary foreslopes in the Bahamas: *Marine Geology*, v. 103, p. 125-136.
- Grammer, G.M., Ginsburg, R.N., and Harris, P.M., 1993, Timing of deposition, diagenesis, and failure of steep carbonate slopes in response to a high-amplitude/high-frequency fluctuation in sea level, Tongue of the Ocean, Bahamas: *American Association of Petroleum Geologists Memoir 57*, p. 107-131.
- Granjeon, D., 2020, Coupled three-dimensional stratigraphic forward and seismic modeling of a Miocene mixed carbonate reservoir, Central Luconia, offshore Malaysia: *in* Rankey, E.C., and Poppelreiter, M., eds., *Cenozoic isolated carbonate platforms- focus southeast Asia*: SEPM (Society of Sedimentary Geologists) Special Publication 114, p. 1-37.
- Handford, C.R., and Loucks, R.G., 1993, Carbonate depositional sequences and systems tracts- responses of carbonate platforms to relative sea-level changes, *in* Loucks, R.G., and Sarg, J.F., eds, *Carbonate sequence stratigraphy: recent developments and applications*: American Association of Petroleum Geologists Memoir 57, p. 3-41.
- Hanebuth, T.J.J., and Stattegger, K., 2004, Depositional sequences on a late Pleistocene-Holocene tropical siliciclastic shelf (Sunda Shelf, southeast Asia): *Journal of Asian Earth Sciences*, v. 12, p. 113-126.
- Janson, X., Eberli, G.P., Bonnafée, F., Gaumet, F., and De Casanove, V., 2007, Seismic expression of a Miocene prograding carbonate margin, Mut Basin, Turkey: *American Association of Petroleum Geologists Bulletin*, v. 91, p. 685-713.

- Kenter, J.A.M., Bracco-Gartner, G.L., and Schlager, W., 2001, Seismic models of a mixed carbonate-siliciclastic shelf margin; Permian upper San Andres Formation, Last Chance Canyon New Mexico: *Geophysics*, v. 66, p. 1744–1748.
- Kosa, E., Warrlich, G.M.E., and Loftus, G., 2015, Wings, mushrooms, and Christmas trees: the carbonate seismic geomorphology of Central Luconia, Miocene – present, offshore Sarawak, northwest Borneo: *American Association of Petroleum Geologists Bulletin*, v. 99, p. 2043-2075.
- Lafranchi, A., Berra, F., and Jadoul, F., 2011, Compositional changes in sigmoidal carbonate clinoforms (Late Tithonia, eastern Sardinia, Italy): insights from quantitative microfacies analyses: *Sedimentology*, v. 58, p. 532-565.
- Makhankova, A., Sautter, B., Mathew, M., Menier, D., and Poppelreiter, M., 2020, Seismic stratigraphy and sedimentology of a Miocene carbonate platform in Luconia, South China Sea: *Geological Journal*, p. 1-17.
- Masaferro, J.L., Bourne, R., and Jauffred, J.C., 2004, Three-dimensional seismic volume visualization of carbonate reservoirs and structures, *in* Eberli, G.P., Masaferro, J.L., and Sarg, J.F., eds., *Seismic imaging of carbonate reservoirs and systems*: American Association of Petroleum Geologists Memoir 81, p. 11-41.
- May, J.A., and Eyles, D.R., 1985, Well log and seismic character of Tertiary Terumbu carbonate, South China Sea, Indonesia: *American Association of Petroleum Geologists Bulletin*, v. 69, p. 1339-1358.
- Mitchum, R.M., Vail, P.R., and Thompson, S., 1977, Seismic stratigraphy and global changes of sea level, part 2: the depositional sequence as a basic unit for stratigraphic analysis: *American Association of Petroleum Geologists Memoir* 26, p. 53-62.

- Neuhaus, D., Borgomano, J., Jauffred, J.C., Mercadier, C., Olotu, S., and Grötsch, J., 2004, Quantitative seismic reservoir characterization of an Oligocene-Miocene carbonate buildup: Malampaya Field, Philippines *in* Eberli, G.P., Masferro, J.L., and Sarg, J.F., eds., *Seismic imaging of carbonate reservoirs and systems: American Association of Petroleum Geologists Memoir 81*, p. 169-183.
- Payton, C.E., 1977, *Seismic stratigraphy: applications to hydrocarbon exploration: American Association of Petroleum Geologists Memoir 26*, p. 1-516.
- Peterson, R.A., Fillippone, W.R., and Coker, F.B., 1955, The synthesis of seismograms from well log data: *Geophysics*, v. 20, p. 516-538.
- Playton, T.E., and Kerans, C., 2015, Late Devonian carbonate margins and foreslopes of the Lennard Shelf, Canning Basin, Western Australia, part B: development during progradation and across the Frasnian-Famennian biotic crisis: *Journal of Sedimentary Research*, v. 85, p. 1362–1392.
- Platford, P.E., 1980, Devonian “Great Barrier Reef” of Canning Basin, Western Australia: *American Association of Petroleum Geologists Bulletin*, v. 64, p. 814-840.
- Ramsayer, G.R., 1979. Seismic stratigraphy, a fundamental exploration tool: 11th Annual Offshore Technology Conference Proceedings, p. 1859-1862.
- Rankey, E.C., 2017, Seismic architecture and seismic geomorphology of heterozoan carbonates: Eocene-Oligocene, Browse Basin, Northwest Shelf, Australia: *Marine and Petroleum Geology*, v. 82, p. 424–443.
- Rankey, E.C., Schlaich, M., Mokhtar, S., Ghon, G., Ali, S.H., and Poppelreiter, M., 2019, Seismic architecture of a Miocene isolated carbonate platform and associated off-shelf

- strata (Central Luconia Province, offshore Malaysia): *Marine and Petroleum Geology*, v. 102, p. 477-495.
- Read, J.F., 1985, Carbonate platform facies models: *American Association of Petroleum Geologists Bulletin*, v. 69, p. 1-21.
- Rendle-Bühning, R., and Reijmer, J., 2005, Controls on grain-size patterns in periself carbonates: marginal setting versus glacio-eustasy: *Sedimentary Geology*, v. 175, p. 99–113.
- Reolid, J., Betzler, C., Braga, J.C., Martin, J.M., Lindhorst, S., and Reijmer, J.J.G., 2014, Reef slope geometries and facies distribution: controlling factors (Messinian, SE Spain): *Facies*, v. 60, p. 737-753.
- Rich, J.L., 1951, Three critical environments of deposition, and criteria for recognition of rocks deposited in each of them: *Geological Society of America Bulletin*, v. 62, p. 1-20.
- Ricker, N., 1953, The form and laws of propagation of seismic wavelets: *Geophysics*, v. 18, p. 10-40.
- Rittenhouse, S., Li, Y., Hughston-Kennedy, K., Fritz, J., Pritchard, J., Cassel, L., Baum, V., Liem, S., and Mooney, T., 2017, Delaware Basin Leonard reservoir characterization, New Mexico and Texas: *Unconventional Resources Technology Conference (URTeC) 2017 Proceedings*, p. 1-22.
- Rosleff-Soerensen, B., Reuning, L., Back, S., and Kukla, P., 2012, Seismic geomorphology and growth architecture of a Miocene barrier reef, Browse Basin, NW-Australia: *Marine and Petroleum Geology*, v. 29, p. 233–254.

- Rudolph, K.W., Schlager, W., and Biddle, K.T., 1989, Seismic models of a carbonate foreslope-to-basin transition, Pico di Vallandro, Dolomites Alps, northern Italy: *Geology*, v. 17, p. 453–456.
- Rudolph, K.W., and Lehmann, P.J., 1989, Platform evolution and sequence stratigraphy of the Natuna Platform, South China Sea, *in* Crevello, P.D., Wilson, J.L., Sarg, J.F., and Read, J.F., eds., *Controls on carbonate and basin development: SEPM (Society of Sedimentary Geologists) Special Publication 44*, p. 353-361.
- Sarg, J.F., 1988, Carbonate sequence stratigraphy, *in* Wilgus, C., ed., *Sea level changes- an integrated approach: SEPM (Society of Sedimentary Geologists) Special Publication 42*, p. 155-181.
- Schlager, W., 1989, Drowning unconformities on carbonate platforms *in* Crevello, P.D., Wilson, J.L., Sarg, J.F., and Read, J.F., eds., *Controls on carbonate and basin development: SEPM (Society of Sedimentary Geologists) Special Publication 44*, p. 15-26.
- Schlager, W., 1991, Depositional bias and environmental change- important factors in sequence stratigraphy: *Sedimentary Geology*, v. 70, p. 109-130.
- Schlager, W., Biddle, K.T., and Stafleau, J., 1991, Picco di Vallandro (Durrenstein)- a platform-basin transition in outcrop and seismic model: *Dolomieu Conference on Carbonate Shelves and Dolomitization, Guidebook Excursion D. Ortisei*, p. 1-22.
- Schlager, W., and Camber, O., 1986, Submarine slope angles, drowning unconformities, and self-erosion of limestone escarpments: *Geology*, v. 14, p. 762-765.
- Schlager, W., Reijmer, J.J.G., and Droxler, A., 1994, Highstand shedding of carbonate platforms: *Journal of Sedimentary Research*, v. 64, p. 270-281.

- Stafleu, J., and Schlager, W., 1993, Pseudo-toplap in seismic models of the Schlern-Raibl contact (Sella Shelf, northern Italy): *Basin Research*, v. 5, p. 55– 65.
- Stafleu, J., Everts, A.J.W., and Kenter, J.A.M., 1993, Seismic models of a prograding carbonate platform: Vercours, south-east France: *Marine and Petroleum Geology*, v. 11, p. 514-527.
- Struckmeyer, H.I.M., Blevin, J.A., Sayers, J., Totterdell., J.M., Baxter, K., and Cathro, D., 1998, Structural evolution of the Browse Basin, North West Shelf: new concepts from deep-seismic data *in* Purcell, P.G., and Purcell, R.R., eds., *The sedimentary basins of western Australia 2: Perth*, Petroleum Exploration Society of Australia Symposium Proceedings, p. 345-366.
- Teillet, T., Fournier, F., Borgomano, J., and Hong, F., 2020a, Origin of seismic reflections in a carbonate gas field, Lower Miocene, offshore Myanmar: *Marine and Petroleum Geology*, v. 113, p. 1-22.
- Teillet, T., Fournier, F., Mantaggioni, L.F., BouDagher-Fadel., M., Borgomano, J., Braga, J.C., Villeneuve, Q., and Hong, F., 2020b, Development patterns of an isolated oligo-mesophotic carbonate buildup, early Miocene, Yadana field, offshore Myanmar: *Marine and Petroleum Geology*, v. 111, p. 440-460.
- Vahrenkamp, V.C., Kamari, Y., and Rahman, S.A., 1998, Three dimensional reservoir geological model and multiple scenario volumetrics of the F23 Miocene carbonate buildup, Luconia Province, offshore Sarawak: *Geological Society of Malaysia Bulletin*, v. 42, p. 15-26.
- Vahrenkamp, V.C., David, F., Duijndam, P., Newall, M., and Crevello, P., 2004, Growth architecture, faulting and karstification of a Middle Miocene carbonate platform, Luconia

- Province, offshore Sarawak, Malaysia: American Association of Petroleum Geologists Bulletin, v. 86, p. 329–350.
- Van Tuyl, J., Alves, T., and Cherns, L., 2018, Geometric and depositional responses of carbonate build-ups to Miocene sea level and regional tectonics offshore northwest Australia: Marine and Petroleum Geology, v. 94, p. 144-165.
- Van Tuyl, J., Alves, T., Cherns, L., Antonatos, G., Burgess, P., and Masiero, I., 2019, Geomorphological evidence of carbonate build-up demise on equatorial margins: A case study from offshore northwest Australia: Marine and Petroleum Geology, v. 104, p. 125-149.
- Van Wagoner, J.C., Posamentier, H.W., Mitchum, R.M., Vail, P.R., Sarg, J.F., Loutit, T.S., and Hardenbol, J., 1988, An overview of the fundamentals of sequence stratigraphy and key definitions: Sea-level changes- an integrated approach: SEPM (Society of Sedimentary Geologists) Special Publication 42, p. 39-45.
- Van Vliet, A., and Krebs, W.N., 2009, The Middle Miocene Unconformity (MMU) in North Luconia, deepwater Sarawak: how unconformable is the unconformity?: Warta Geologi, v. 35, p. 130-132.
- Ward, R.F., Kendall, C.G.S.C., and Harris, P.M., 1986, Upper Permian (Guadalupian) facies and their association with hydrocarbons- Permian Basin, West Texas and New Mexico: American Association of Petroleum Geologists Bulletin, v. 70, p. 239-262.
- Warrlich, G.M.D., Bosence, D., Waltham, D., Wood, C., Boylan, A., and Badenas, B., 2008, 3D stratigraphic forward modelling for analysis and prediction of carbonate platform stratigraphies in exploration and production: Marine and Petroleum Geology, v. 25, p. 25-58.

- Warrlich, G.M.D., Taberner, C., Asyee, W., Stephenson, B., Esteban, M., Boya-Ferrero, M., Dombrowski, A., and Van Konijnenburg, J.H., 2010, The impact of postdepositional processes on reservoir properties: two case studies of tertiary carbonate buildup gas fields in southeast Asia (Malampaya and E11): Cenozoic carbonate systems of Australasia: SEPM (Society of Sedimentary Geologists) Special Publication 95, p. 99-127.
- Warrlich, G.M.D., Adams, E.W., Ryba, A., Tam, T., Ting, K.K., and Tang, H.K., 2019, What matters for flow and recovery in carbonate gas reservoirs: insights from the mature Central Luconia Province, offshore Sarawak, Malaysia: American Association of Petroleum Geology Bulletin, v. 103, p. 691-721.
- Widess, M.B., 1973, How thin is a thin bed?: Geophysics, v. 38, p. 1176-1180.
- Wylie, M.R.J., Gregory, A.R., and Gardner, L.W., 1956, Elastic wave velocities in heterogeneous and porous media: Geophysics, v. 21, p. 41-70.
- Yose, L.A., Ruf, A.S., Strohmenger C.J., Schuelke J.S., Gombos, A., Al-Hosani, I., Al-Maskary, G., Bloch, S., Al-Mehairi, A., and Johnson, I.G., 2006, Three dimensional characterization of a heterogeneous carbonate reservoir, Lower Cretaceous, Abu Dhabi (United Arab Emirates), *in* Harris, P.M., and Weber, L.J., eds., Giant hydrocarbon reservoirs of the world: from rocks to reservoir characterization and modeling: American Association of Petroleum Geologists Memoir 88, p. 173– 212.
- Zampetti, V., Schlager, W., van Konijnenburg, J.H., and Everts, A.J., 2003, Depositional history and origin of porosity in a Miocene carbonate platform of central Luconia, offshore Sarawak: Geological Society of Malaysia Bulletin, v. 47, p. 139-152.

Zampetti, V., Schlager, W., van Konijnenburg, J.H., and Everts, A.J., 2004, Architecture and growth history of a Miocene carbonate platform from 3D seismic reflection data; Luconia province, offshore Sarawak, Malaysia: *Marine and Petroleum Geology*, v. 21, p. 517-534.

Figures

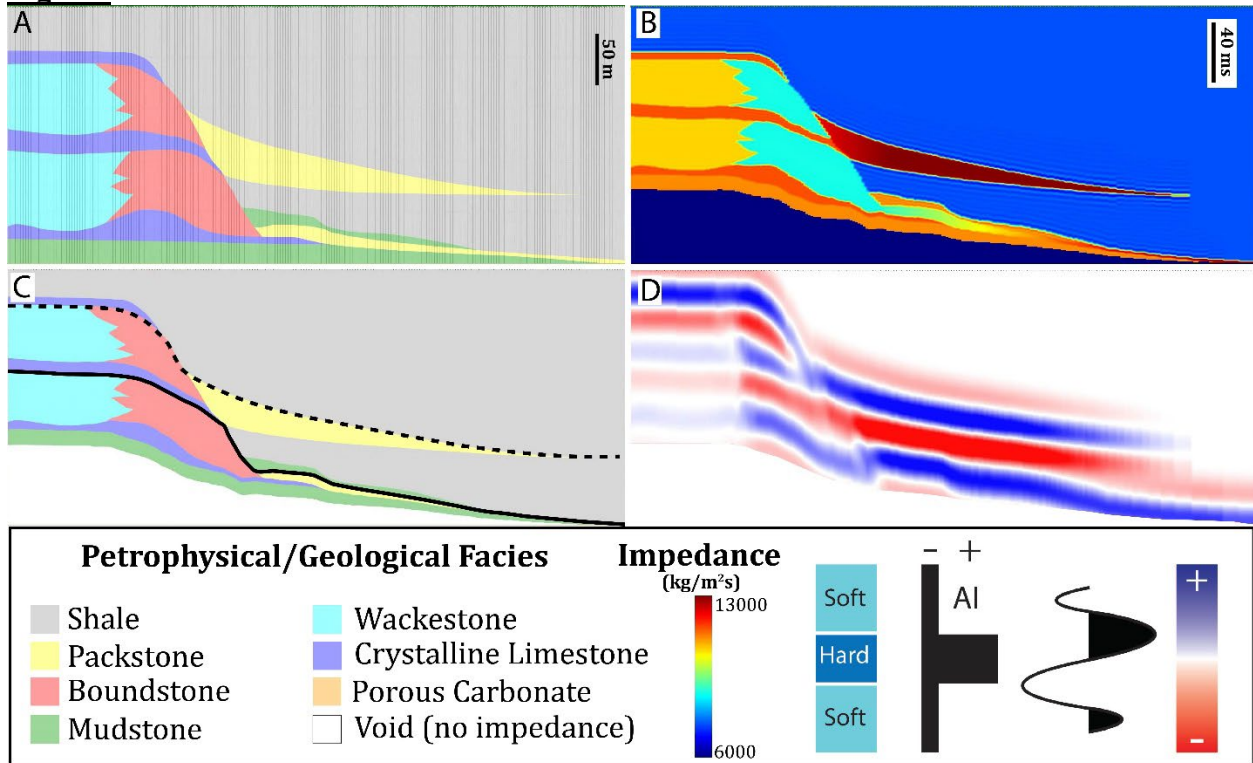


Figure 1: Diagram illustrating a representative geologic conceptual model to seismic model workflow. A) Facies schematic model displayed in depth wherein facies are based on Dunham classifications or rock composition (shale only). B) Acoustic impedance volume in the time domain, assuming facies-based velocity and density. C) Facies schematic converted to time, using velocities in B, with sequence boundaries superimposed. And D) synthetic seismic volume generated by convolving the reflectivity facies model derived from the impedance volume with a Ricker wavelet. Horizontal scale in this and subsequent figures are not labelled, because carbonate margin gradients can vary greatly. In all scenarios, left is shelfward and right is basinward.

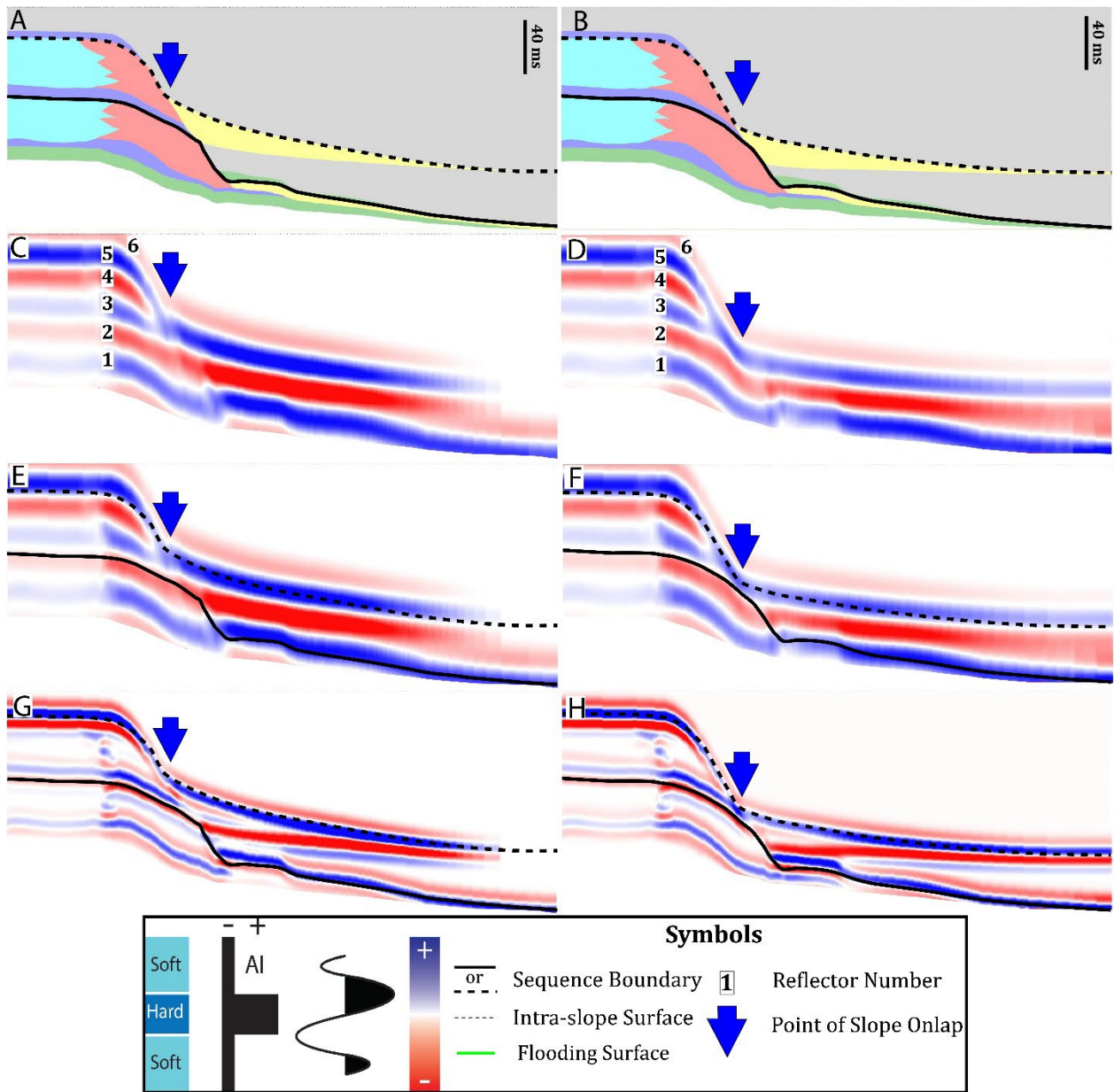


Figure 2: Geological facies and seismic models for the Base and High-Relief Bypass scenarios from the Aggrading Shelf Margin Slope suite of models. A-B) Geological facies models for the Base (A) and High-Relief Bypass (B) slope scenarios in time. C-D) 22 Hz seismic models for the Base (C) and High-Relief Bypass (D) slope scenarios. Reflectors discussed in text are numbered, from oldest to youngest. E-F) 22 Hz seismic model for the Base (E) and High-Relief Bypass (F) scenarios with sequence boundaries marked by the solid and dashed black lines, and updip-most margin point of slope onlap is denoted with a blue arrow. G-F) 60 Hz seismic models for the Base (G) and High-Relief Bypass (H) scenarios with sequence boundaries and the point of slope onlap superimposed. Key to geological facies same as Figure 1. See text for additional discussion.

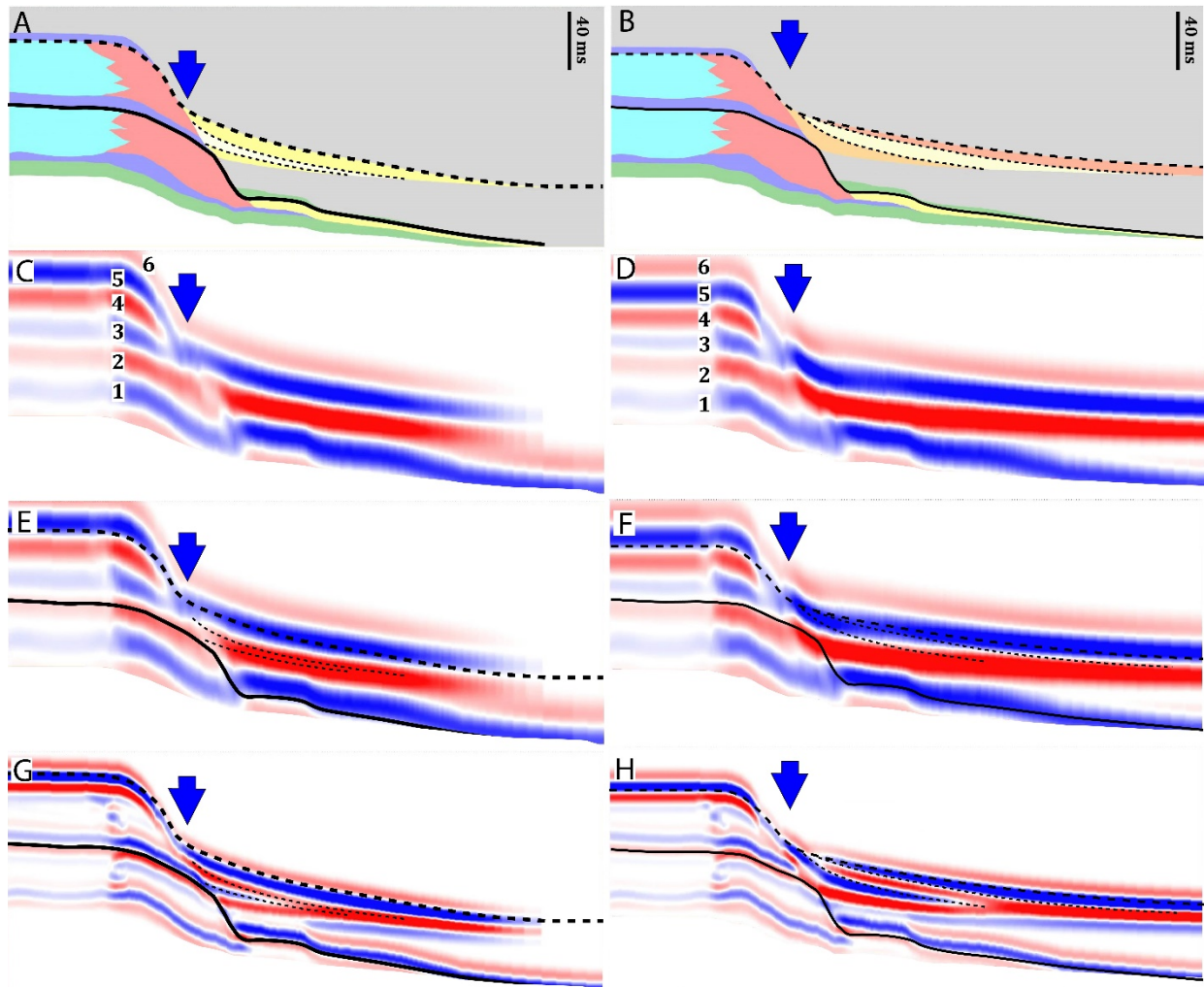


Figure 3: Geological facies and seismic models for the Three Layer Onlapping and Three Layer Offlapping scenarios of the Aggrading Shelf Margin Slope suite. A-B) Geological facies models for the Three Layer Onlapping (A) and Three Layer Offlapping (B) scenarios. C-D) 22 Hz seismic models for the Three Layer Onlapping (C) and Three Layer Offlapping (D) scenarios. Reflectors discussed in text are numbered. E-F) 22 Hz seismic models for the Three Layer Onlapping (E) and Three Layer Offlapping (F) scenarios with sequence boundaries and the point of slope onlap superimposed. G-H) 60 Hz seismic models for the Three Layer Onlapping (G) and Three Layer Offlapping scenarios with sequence boundaries and point of slope onlap superimposed. Key to geological facies, seismic character, and interpretation same as Figure 1. Note that the 22 Hz models demonstrate only subtle differences in seismic character between onlapping and offlapping geometries. See text for detailed discussion.

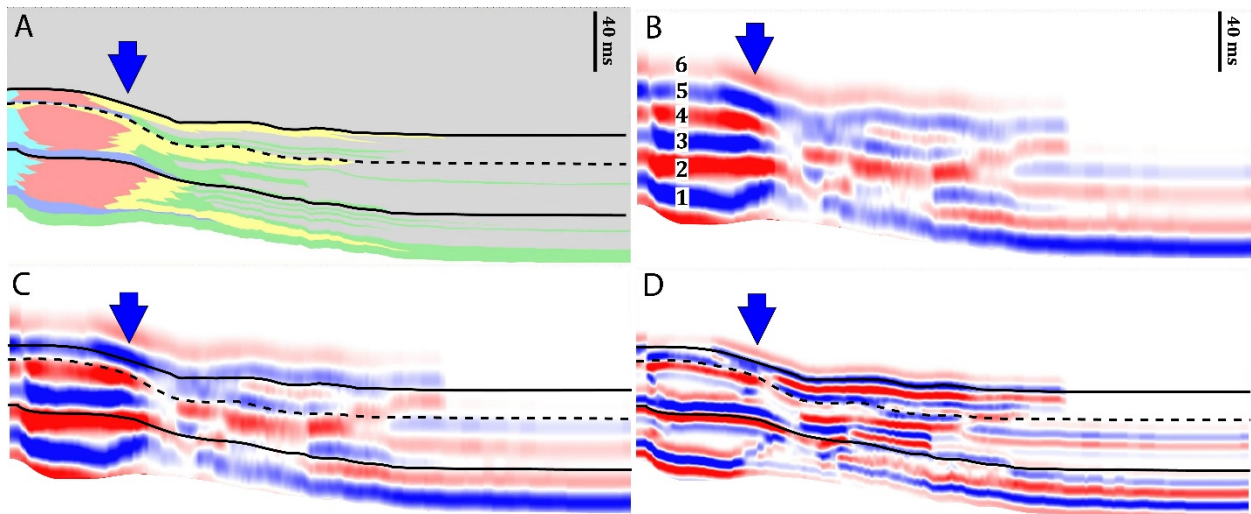


Figure 4: Geological facies and seismic models of the Low-Relief Interfingering scenario. A) Geological facies model for the Low-Relief Interfingering deposit scenario. B) 22 Hz seismic model for the Low-Relief Interfingering slope deposit scenario. Reflectors discussed in text are numbered. C) 22 Hz seismic model for the Low-Relief Interfingering slope deposit scenario with sequence boundaries and the point of onlap annotated. D) 60 Hz seismic model for the Low-Relief Interfingering scenario. Key to geological facies, seismic character, and interpretation are the same as in Figure 1. Both the 22 Hz and 60 Hz seismic models illustrate some of the seismic ambiguity possible in low depositional relief scenarios. See text for detailed discussion.

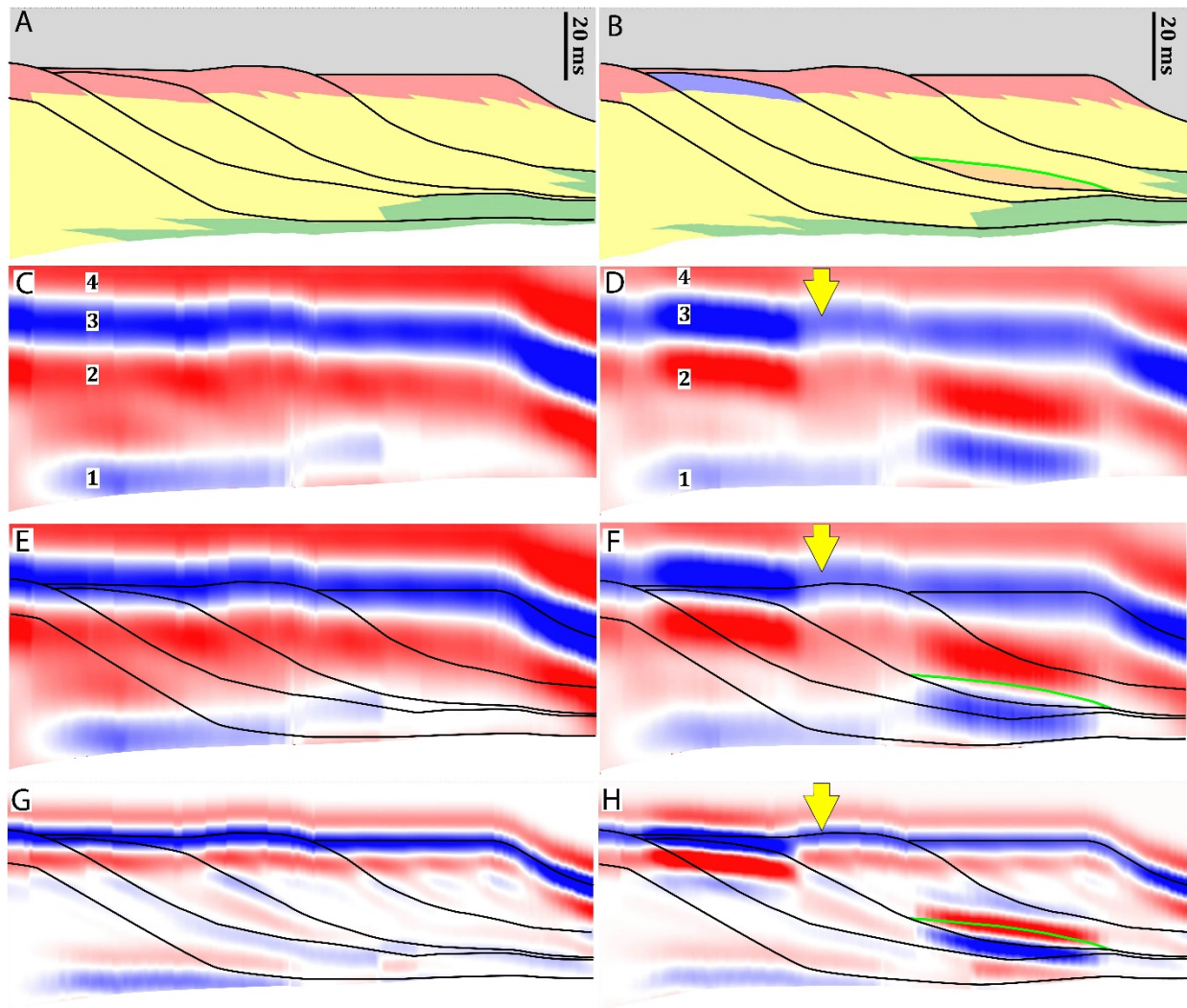


Figure 5. Geological facies and seismic models for the Base and Toe of Slope Lowstand scenarios in the Prograding Shelf Margin suite. A-B) Geological facies models for the Base (A) and Toe of Slope Lowstand (B) scenarios. C-D) Uninterpreted 22 Hz seismic models of the Base (C) and Toe of Slope Lowstand scenarios. Reflectors discussed in text are numbered. E-F) 22 Hz seismic models of the Base (E) and Toe of Slope Lowstand scenarios, with sequence boundaries and flooding surfaces superimposed. G-H) 60 Hz seismic models for the Base (G) and Toe of Slope Lowstand scenario. Key to geological facies, seismic character, and interpretation are the same as in Figure 1. The Toe of Slope Lowstand model (D) demonstrates that intervals within a facies with higher or lower acoustic impedance values result in changes in reflector amplitude relative to that of the Base Model (C). See text for further discussion.

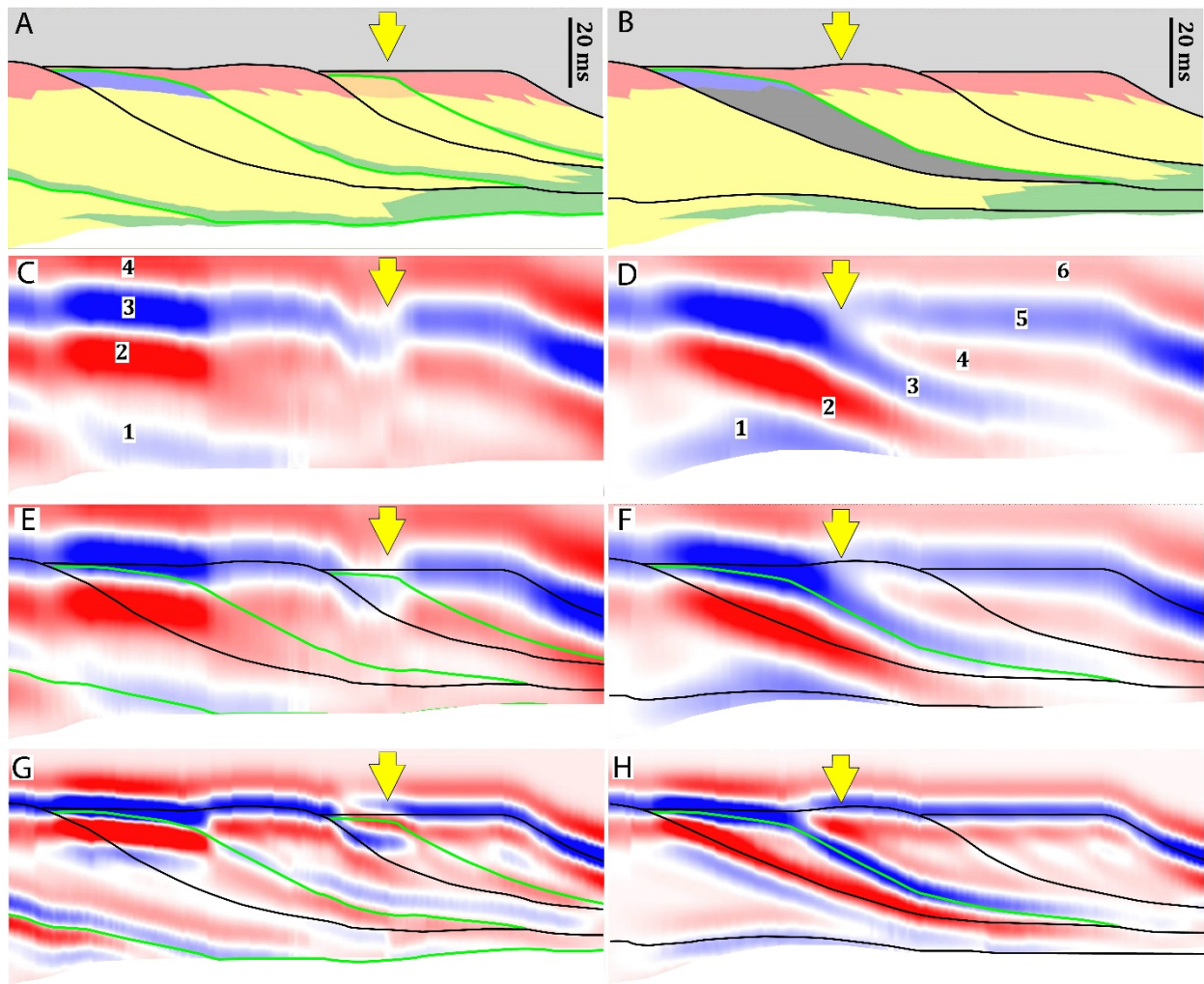


Figure 6: Geological facies and seismic models for the Flooding Interval and Tight Clinoform scenarios. A-B) Geological facies models for the Flooding Interval (A) and Tight Clinoform (B) scenarios. C-D) Uninterpreted 22 Hz seismic models of the Flooding Interval (C) and Tight Clinoform Lowstand scenarios. Reflectors discussed in text are numbered, and a point of apparent onlap is marked by the yellow arrow. E-F) 22 Hz seismic models of the Flooding Interval (E) and Tight Clinoform scenarios, with sequence boundaries and flooding surfaces superimposed. G-H) 60 Hz seismic models for the Flooding Intervals (G) and Tight Clinoform scenario. Key to geological facies, seismic character, and interpretation are the same as in Figure 1. The 22 Hz seismic models (C and D) demonstrate the level of detail retained in slope deposits and that different geological scenarios (e.g. a low-impedance interval in the reef facies, and a high-impedance transgressive reef-slope interval) can produce similar seismic geometries. See text for further discussion.

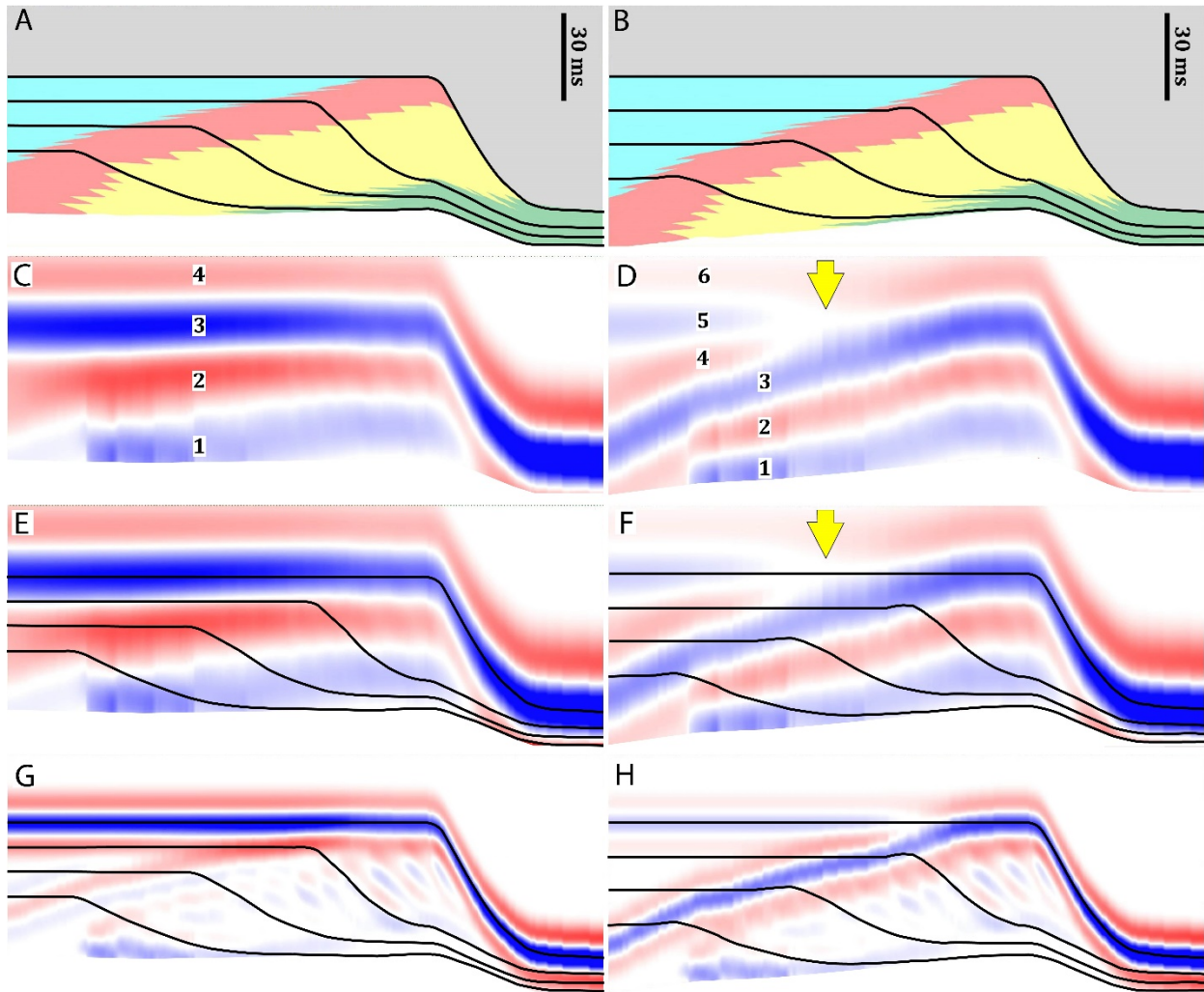


Figure 7: Geological facies and seismic models for the Combination Prograding and Aggrading suite of models. A-B) Geological models for the (A) High-Impedance Interior (HIMI) and (B) Low-Impedance Interior (LIMI) scenarios. Note that the geometries are identical, but the interior of the high-impedance model, which includes higher velocity, appears thinner because these sections are in time. C-D) Uninterpreted 22 Hz seismic models for the HIMI (C) and the LIMI (D) scenarios. Reflectors described in the text are numbered. E-F) 22 Hz seismic models for the HIMI (E) and LIMI (F) scenarios with time lines superimposed. G-H) 60 Hz seismic models for the HIMI (G) and LIMI (H) scenarios. Key to geologic facies, seismic character, and interpretation are the same as Figure 1. Both 22 Hz models (C & D) illustrate the critical role which interior acoustic impedance values plays in the seismic expression of a carbonate shelf margin. See text for detailed description.

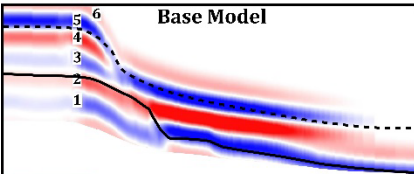
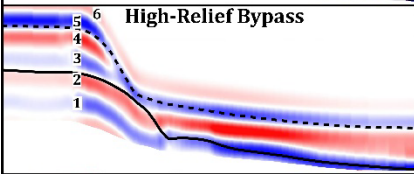
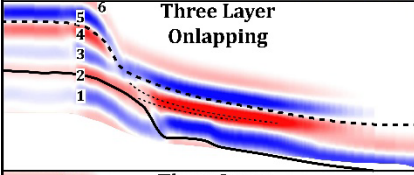
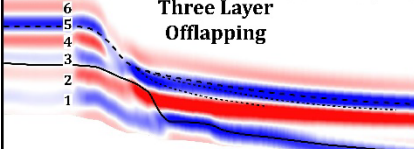
Model	Observations	Interpretations
 <p>Base Model</p>	<p>1) Decrease in amplitude, increase in loop duration in reflectors 2, 3, & 5 at the point of slope onlap</p>	<p>1) Changes in a reflectors character (amplitude, loop duration, & geometry) can suggest a change in facies or petrophysical properties</p>
 <p>High-Relief Bypass</p>	<p>2) No break in continuity in reflectors 1, 4, & 5 despite lateral changes in facies</p>	<p>2) Geologic complexity within slope deposits has no appreciable influence on their seismic character when complexity is beneath seismic resolution</p>
 <p>Three Layer Onlapping</p>	<p>3) Lower sequence boundary deviates from reflector 2 at the platform margin</p>	<p>3) Time lines can cut across reflectors, and vice versa</p>
 <p>Three Layer Offlapping</p>	<p>4) Upper sequence boundary deviates from reflector 3/5 basinward where slope deposits thin out</p>	

Figure 8: List of four observations and three interpretations regarding the seismic character and sequence boundaries of all four seismic models in the aggrading shelf margin suite of models. Interpretation 1 relates to observations 1 and 2, interpretation 2 relates to the intra-slope layers of the Three Layer Onlapping and Offlapping models, and interpretation three relates to observations 3 and 4.

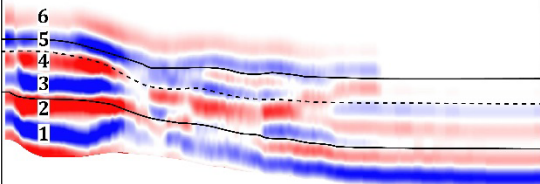
Model	Observations	Interpretations
<p data-bbox="342 226 576 254">Low-Relief Interfingering</p> 	<p data-bbox="732 226 1073 338">1) Reflectors are mostly horizontal and continuous across the model, but lose amplitude at the margin</p> <p data-bbox="732 344 1073 436">2) Sequence boundaries deviate from reflectors from platform to basin</p>	<p data-bbox="1078 226 1414 338">1) Low platform-basin relief produces ambiguity in the lateral extent of reef, slope, and basinal strata</p> <p data-bbox="1078 344 1414 436">2) Sequence boundaries deviate from reflectors due to facies changes</p>

Figure 9: List of two observations and two interpretations regarding the seismic character and sequence boundaries of the Low-Relief Interfingering model. Interpretation 1 relates to observation 1 and the ambiguity described in the text. Interpretation 2 relates to observation 2.

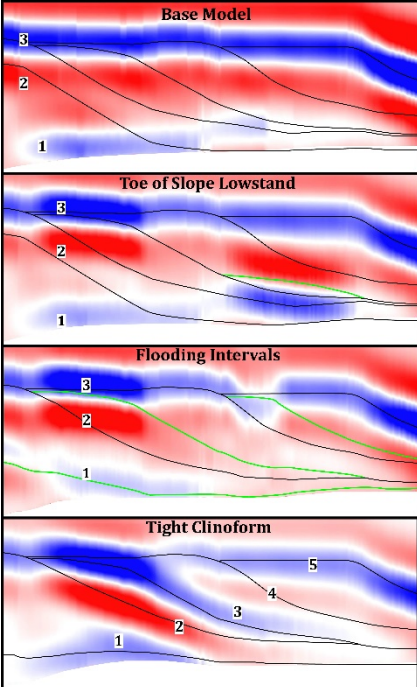
Model	Observations	Interpretations
 <p>Base Model</p> <p>Toe of Slope Lowstand</p> <p>Flooding Intervals</p> <p>Tight Clinoform</p>	<p>1) In the ToS Lowstand, Flooding Interval, and TST Clinoform models, amplitude increases in petrophysically distinct intervals (i.e., cemented or porous reef deposits; porous lowstand deposits)</p> <p>2) Low-impedance intervals in a reef (Figure 8C) and a high-impedance clinoform (Figure 8D) scenarios produce similar geometries</p> <p>3) The Base and Toe of Slope Lowstand models both contain horizontal, parallel reflectors</p> <p>4) Some reflectors cut across time lines, and some time lines cut across reflectors</p>	<p>1) Changes in a continuous reflector's character (amplitude, loop duration, and geometry) can suggest a change in facies or petrophysical properties</p> <p>2) Petrophysical anomalies in reef facies on their own can produce onlapping reflector terminations. Geometries are similar to larger, more geologically significant events</p> <p>3) Low-frequency data obscures much of the detail in a prograding system, most notably sequence boundaries and clinoforms. Only high-contrast interfaces (i.e., the tight clinoform) are resolved</p>

Figure 10: List of four observations and three interpretations regarding the seismic character and sequence boundaries of all four seismic models in the prograding shelf margin suite of models. Interpretation 1 relates to observation 1, interpretation 2 relates to observation 2, and interpretation 3 relates to observations 3 and 4.

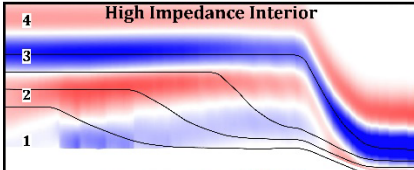
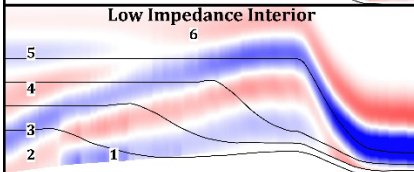
Model	Observations	Interpretations
 <p>High Impedance Interior</p>	<p>1) 4 reflectors in the HIPI, 6 in the LIPI</p> <p>2) Interior portion of all HIPI reflectors are horizontal and parallel</p> <p>3) Interior portions of LIPI reflectors 1, 2, and 3 dip shelfward; reflectors 4, 5, and 6 are parallel and horizontal</p>	<p>1) Impedance contrasts between facies plays a critical role in the seismic expression of carbonate margins</p> <p>2) Low-frequency data obscures geological variability and in some cases produces pseudo-unconformities</p>
 <p>Low Impedance Interior</p>	<p>4) Reflectors 4 and 5 of the LIPI onlap reflector 3</p> <p>5) Reflector amplitude & loop duration increase basinward of the shelf margin in both the HIPI and LIPI</p>	<p>3) Reflectors can cut across time lines, and vice versa</p> <p>4) Changes in reflector character (amplitude, loop duration, and geometry) suggest lateral changes in facies</p>

Figure 11 List of four observations and three interpretations regarding the seismic character and sequence boundaries of all four seismic models in the combination prograding and aggrading shelf margin suite of models. Interpretation 1 derives from observations 1, 2, and 3. Interpretation 2 derives from observation 4. Interpretation 3 derives from observations of cross-cutting relationships between time lines and seismic reflectors in both models. Interpretation 4 derives from observation 5.

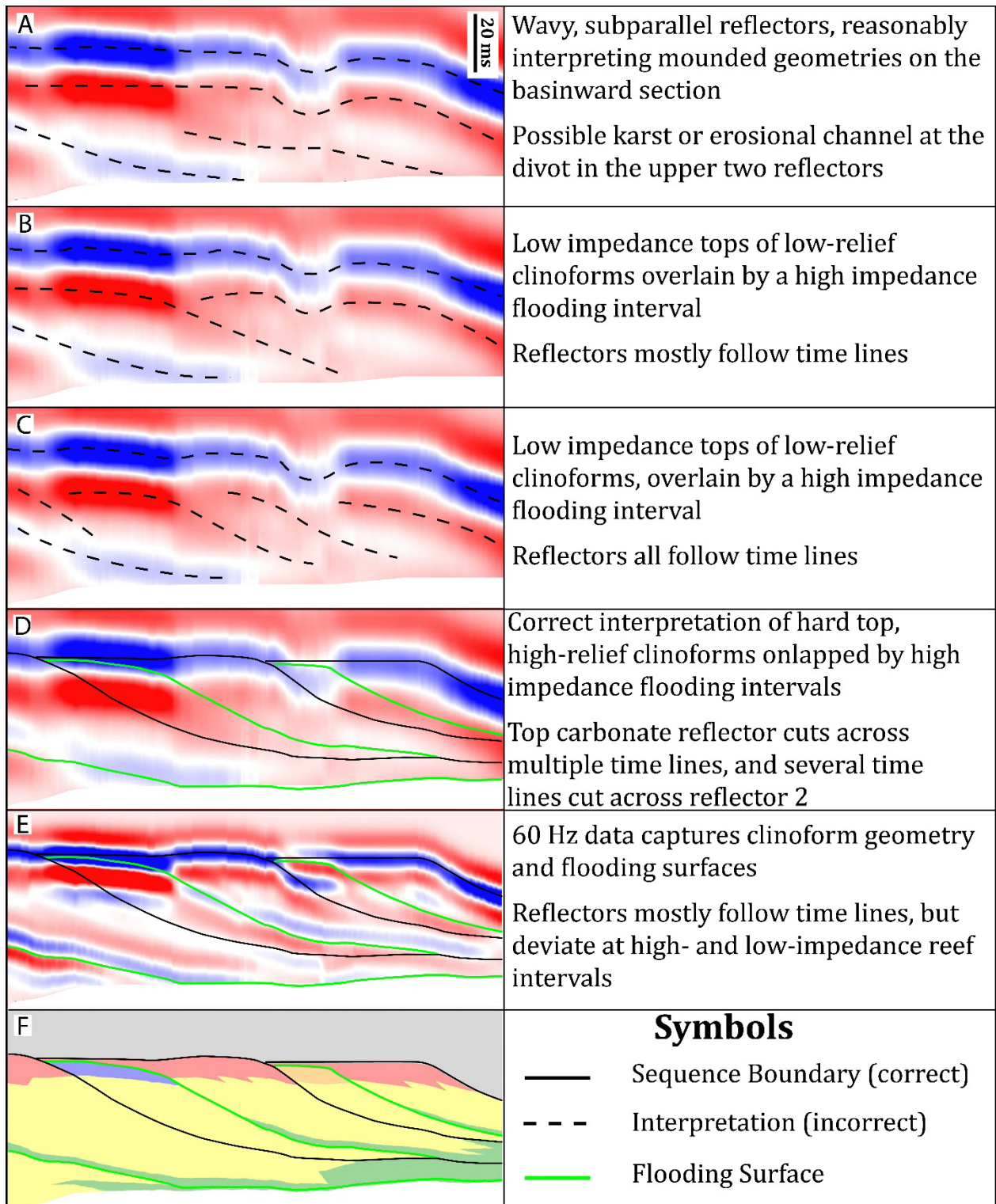


Figure 12: Plausible, but incorrect, and correct interpretations of the Flooding Interval scenario from the Prograding Shelf Margin suite of models. A-C) Plausible, but incorrect interpretations of the 22 Hz seismic model of the Flooding Interval scenario. Text boxes to the right of each interpretation describe what the incorrect interpretation is, and how that interpretation relates reflectors to time lines (flooding surfaces and sequence boundaries). D) Correct interpretation of

the 22 Hz seismic model from the Flooding Interval scenario. E) Correct interpretation of the 60 Hz seismic model. And F) the geologic facies model for the Flooding Interval scenario, with sequence boundaries and flooding surfaces superimposed. Key to geological facies are the same as Figure 1. See text for further discussion.

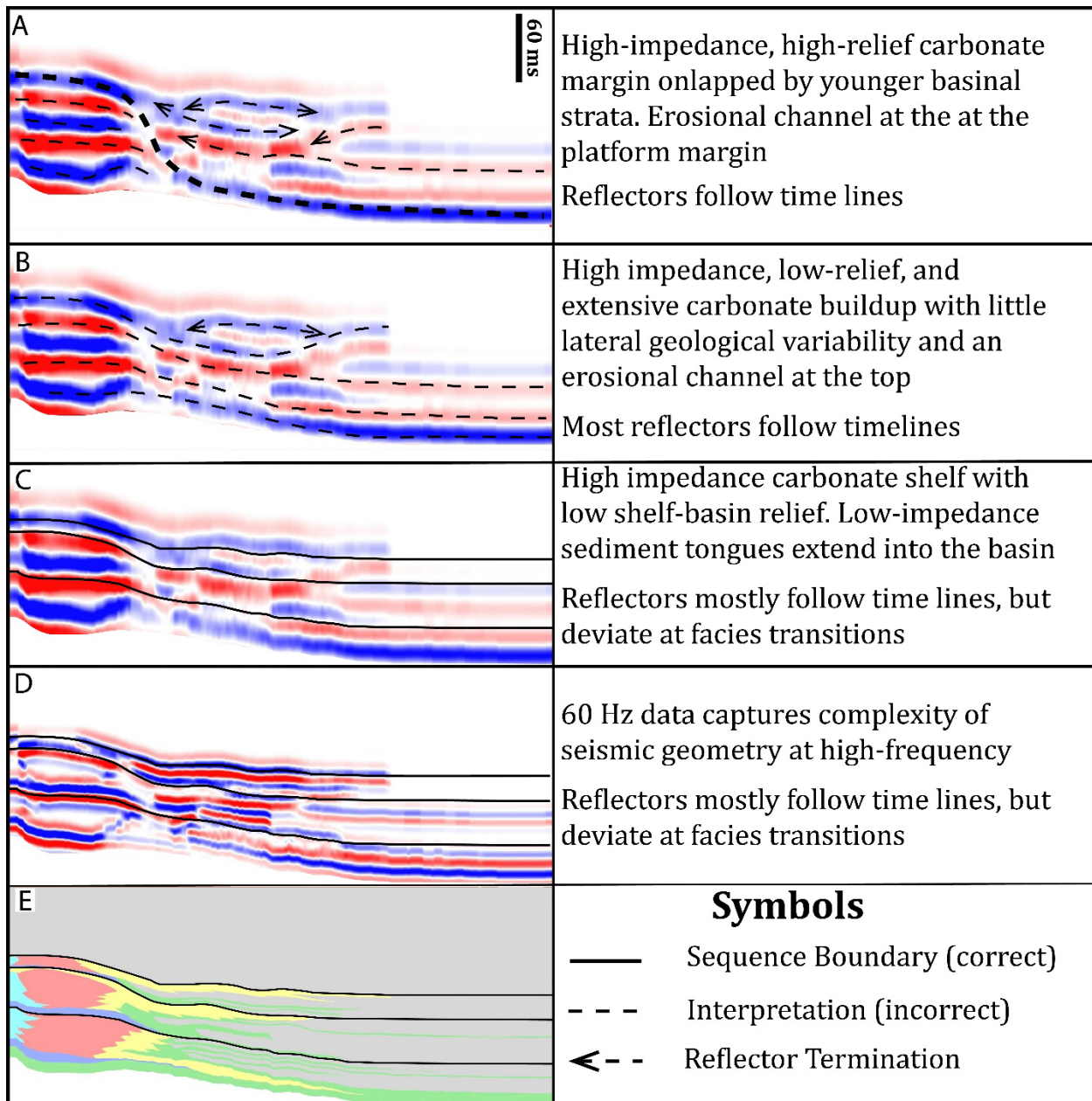


Figure 13: Plausible, but incorrect and correct interpretations of the Low-Relief Interfingering scenario. A-B) Plausible, but incorrect interpretations of the 22 Hz seismic model of the Low-Relief Interfingering scenario. Text boxes to the right of each incorrect interpretation describe what the incorrect interpretation is, and how that interpretation relates reflectors to time lines (flooding surfaces and sequence boundaries). C) Correct interpretation of the 22 Hz seismic model from the Low-Relief Interfingering scenario. D) Correct interpretation of the 60 Hz seismic model. And E) the geologic facies model for the Low-Relief Interfingering scenario, with sequence boundaries superimposed. Note how the simple seismic character belies the geological complexity of the scenario, even with a 60 Hz wavelet. Key to geological facies are the same as Figure 1. See text for further discussion.

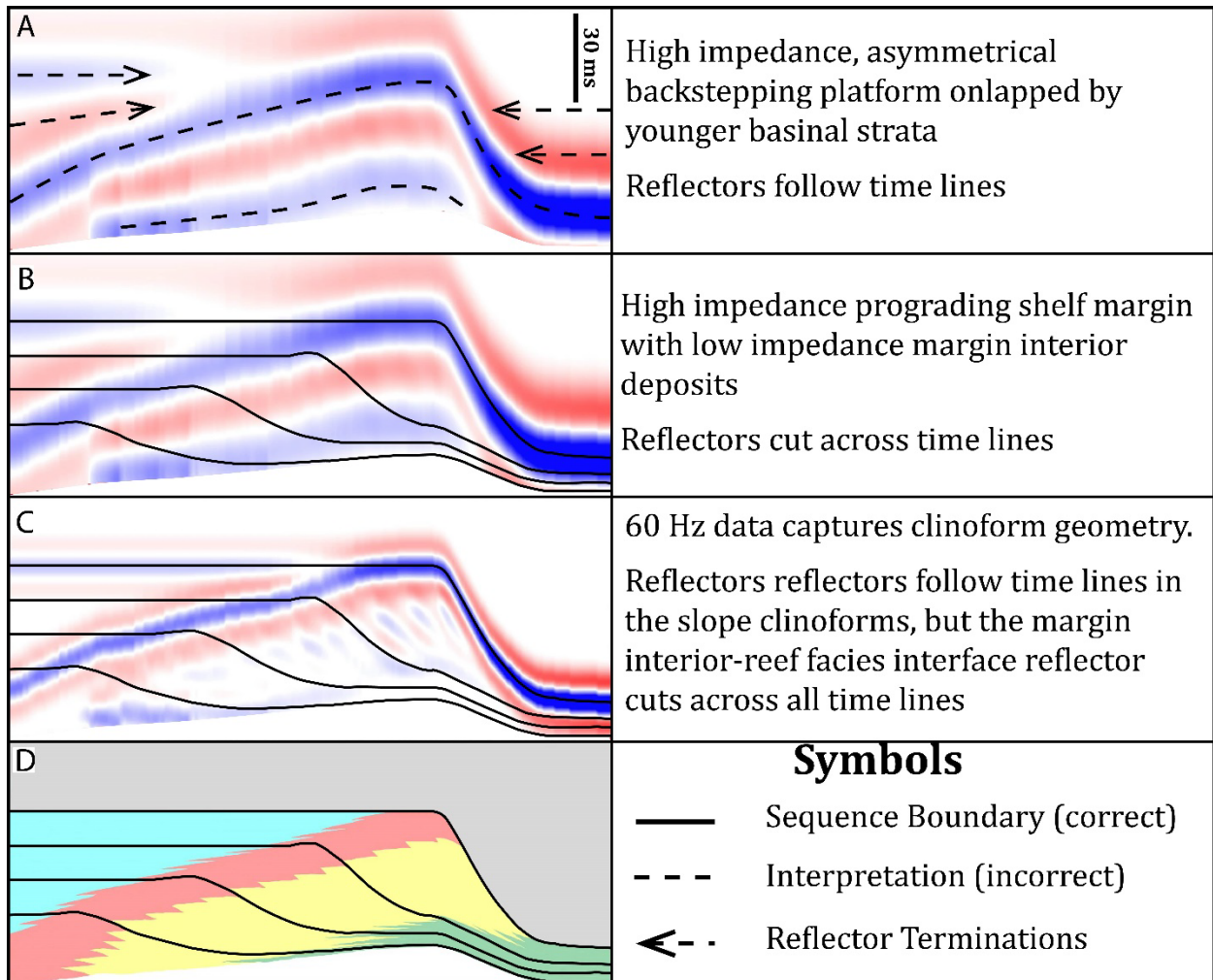


Figure 14: Plausible, but incorrect and correct interpretations of the Low-Impedance Margin Interior (LIMI) scenario. (A) A plausible, but incorrect interpretation of the 22 Hz seismic model of the LIMI scenario. (B) The correct interpretation of the 22 Hz LIM I model. (C) Correct interpretation of the 60 Hz LIM I seismic model. And (D) geological facies model for the LIM I scenario. Key to geological facies are the same as Figure 1. Note how the margin interior reflectors onlap the margin interior-reef facies interface, producing a pseudo-unconformity. See text for further discussion.

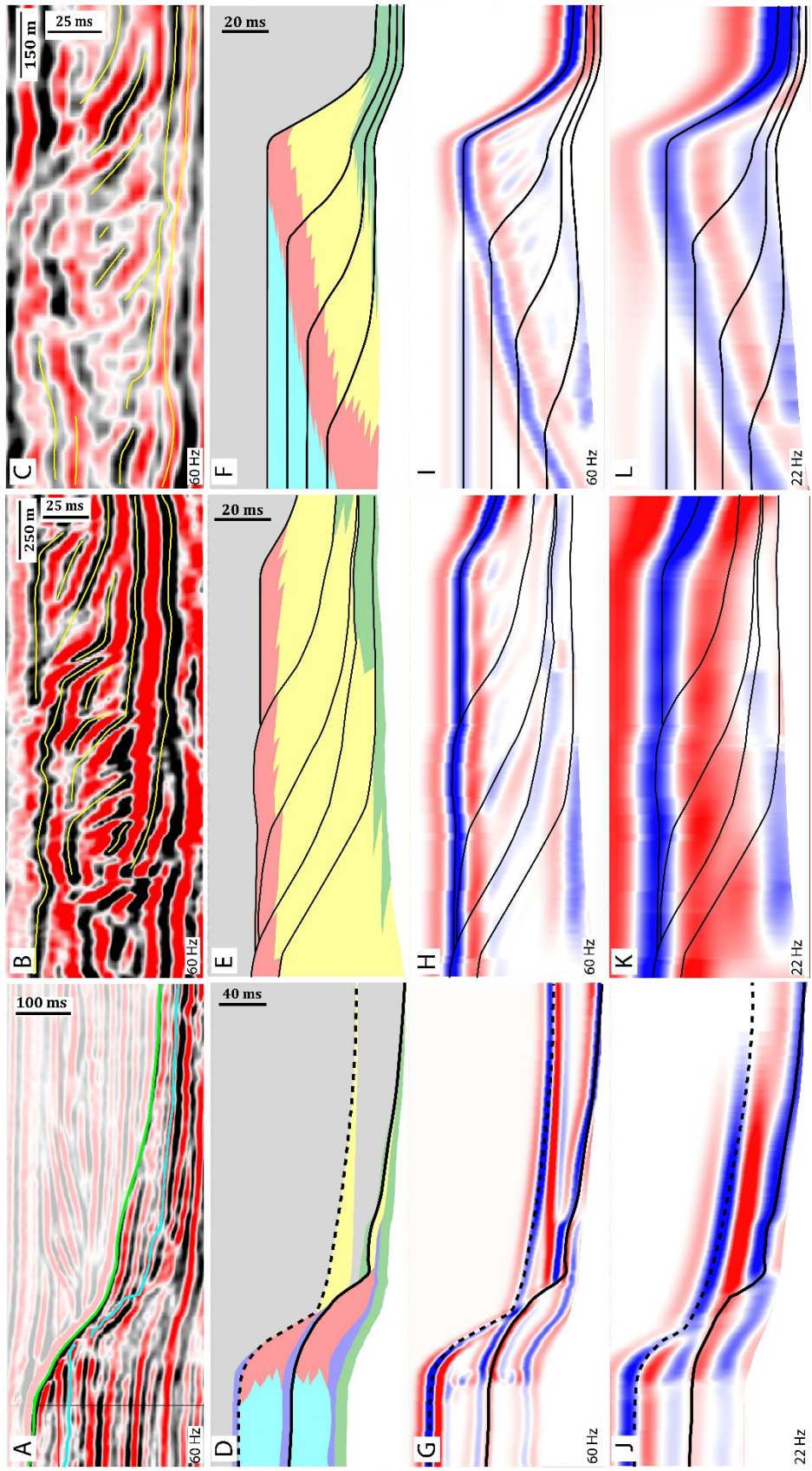


Figure 15: High-frequency (60 Hz) seismic figures from Browse Basin, Australia, some of which served as inspiration for three endmember geometries. A-C) 60 Hz seismic examples of an aggrading carbonate margin (A), prograding carbonate margin (B), and combination aggrading and prograding carbonate Margin (C). D-F) facies models of the High-Relief Bypass Slope Deposits (D), Base Prograding (E) and Combination Prograding and Aggrading (F) model sets. G-H) 60 Hz seismic models for the High-Relief Bypass Slope Deposits (G), Base Prograding (H), and Combination Prograding and Aggrading (I) scenarios. J-L) 22 Hz seismic models of the High-Relief Bypass Slope Deposits (J), Base Prograding (K), and Combination Prograding and Aggrading (L) scenarios. The objective of this exercise was not directly reproducing these seismic data. Rather, the purpose was to illustrate how geological detail is obscured in low-frequency data. Note the significant decrease in the number and complexity of reflectors between the 60 Hz data and models and the 22Hz models. Key for geological facies, seismic character, and interpretation are the same as Figures 1 and 2. See text for additional discussion.

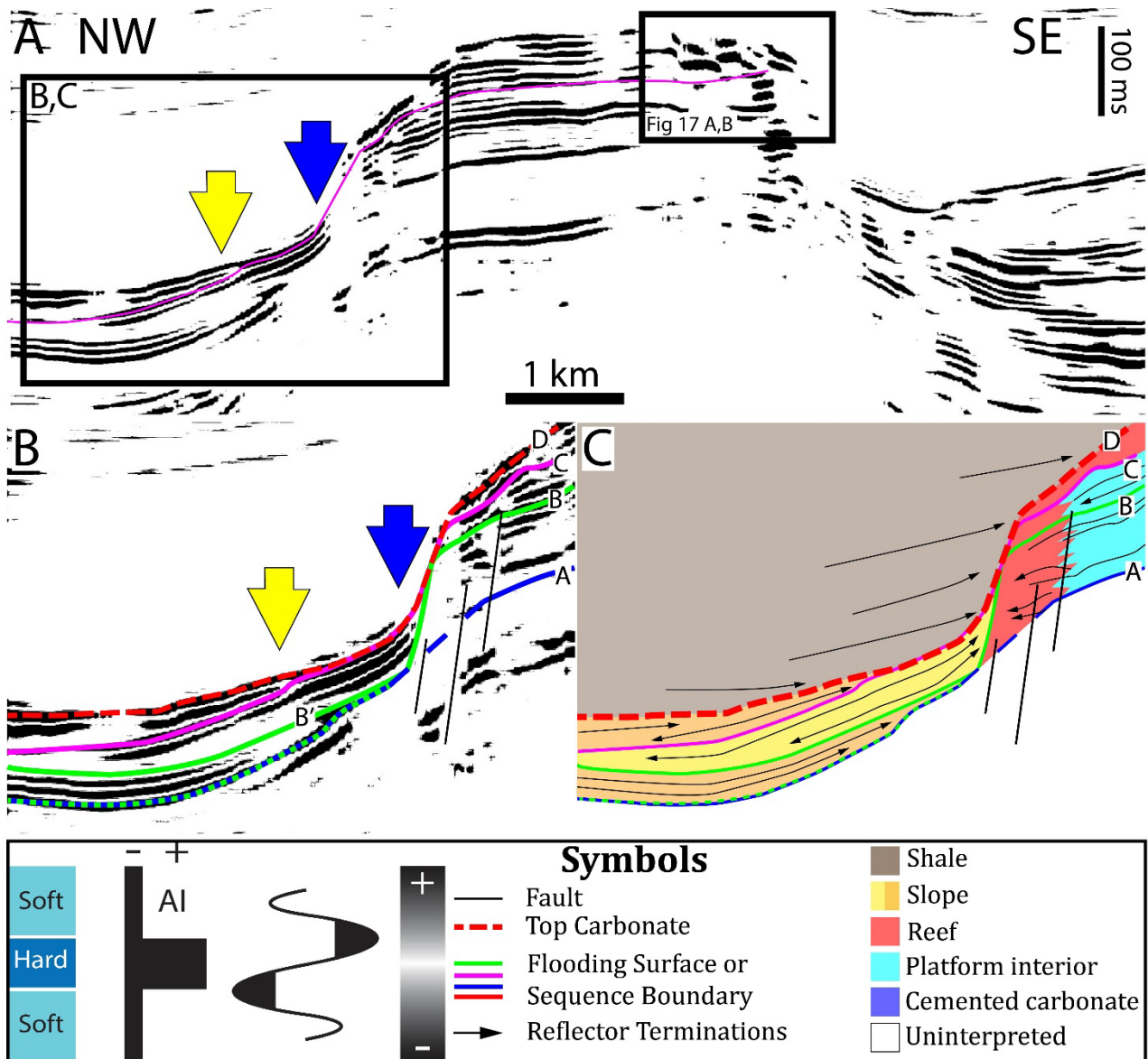


Figure 16: Example of applying model insights to real-world seismic data from Platform FX. A) Seismic line of Platform FX from Central Luconia, offshore Borneo, Malaysia. B) Close-up of the northwestern platform margin, annotated with sequence boundaries, flooding surfaces, and faults. Yellow and blue arrows indicate points of interest discussed in the text. C) Interpretive line sketch of part B, with reflector terminations and geologic facies interpretations. Note the change of reflector amplitude and geometry at the blue arrow is interpreted as a facies change, and onlap at the yellow arrow is interpreted as a second slope body offlapping older slope deposits. See text for additional discussion.

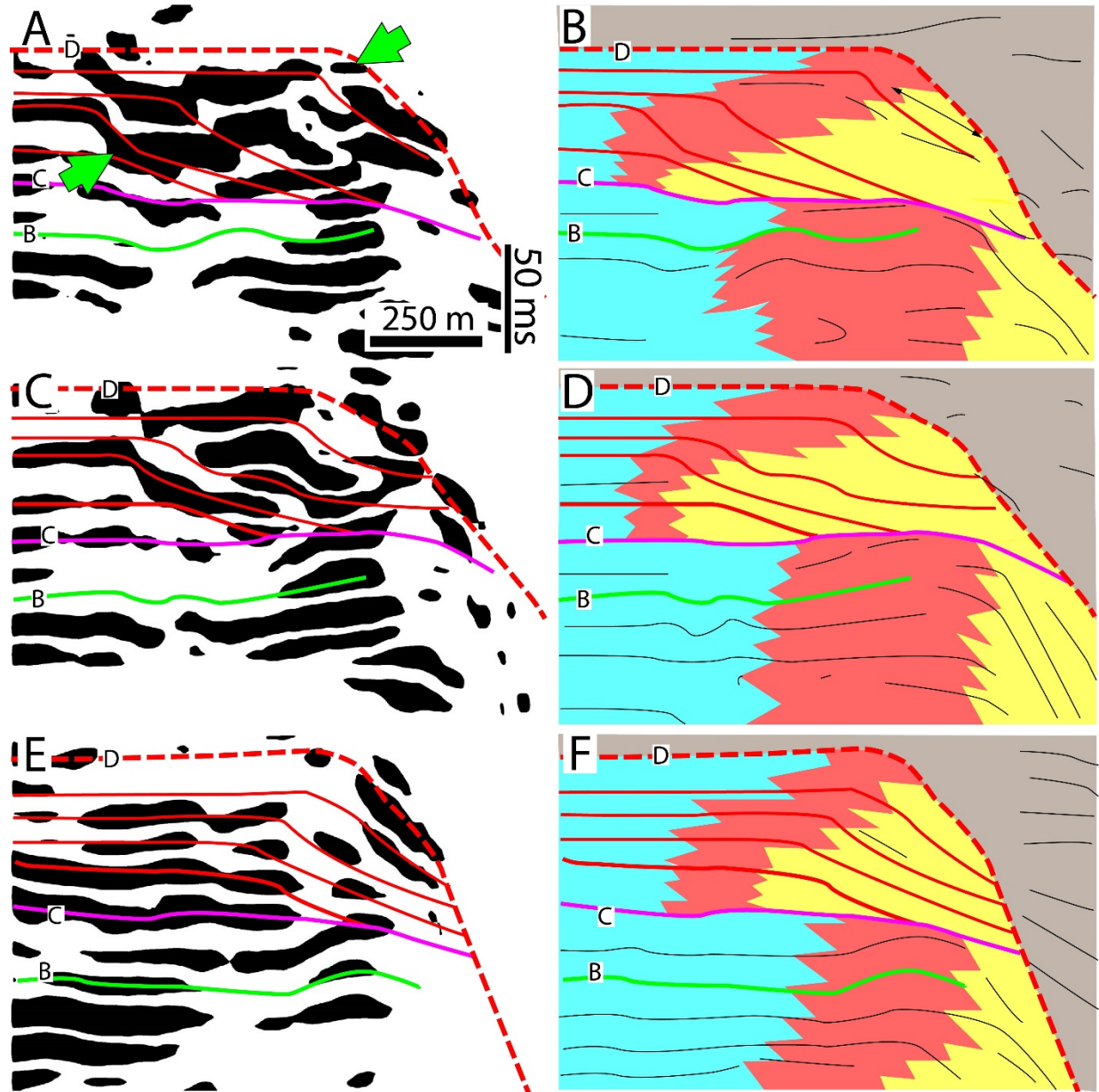


Figure 17: Second example of applying insights from the models to interpret Platform FX. A-B) Close-up of southeastern margin of Platform FX (A) and associated line sketch interpretation (B) from Figure 16A, with sequence boundaries and flooding surfaces superimposed. C-D) A second seismic data (C) and line sketch (D) pair from Platform FX's southeastern margin approximately one kilometer to the southwest of A and B. E-F) A third seismic data (E) and line sketch (F) pair from Platform FX's southeastern margin approximately two kilometers to the northwest of A and B. Consistent reflector geometries across several seismic figures support an interpretation of a prograding and slightly aggrading carbonate platform margin. Key to geological facies, seismic character, and interpretation are the same as Figure 16. See text for additional discussion.

Tables

Lithology	V_P (m/s)	ρ (g/cm³)
Boundstone	4125	2.35
Packstone -Wackestone	3750-6000 4000-6500 4750-6000	2.35
Crystalline Carbonate	5000	2.60
Grainstone	3250	2.35
Wackestone	3250 4500	2.40
Carbonate Mudstone	4700	2.40
Shale	3000	2.30

Table 1: Petrophysical properties of each facies for models. Most facies are assigned one P-wave velocity (V_P) and density (ρ). Velocity is varied within slope deposits, however, to simulate lateral sedimentological and petrophysical differences with increasing distance from the shelf margin.

Model	Description	Variable(s) Tested	Inspiration/Examples
Base	Control model. One-layer slope deposit which onlaps the platform margin	N/A	Seismic data from Browse Basin, NW Australia (Rankey, personal communication) Quaternary deposits, Maldives (Betzler et al., 2016)
High-Relief Bypass	Identical slope geometry and thickness as the Base model, but with greater platform-basin relief	Platform-basin relief	Devonian reef deposits, Canning Basin, Western Australia (Playford, 1980) Quaternary slope deposits, Tongue of the Ocean, Bahamas (Grammer and Ginsburg, 1992)
Three Layer Onlapping	Three stacked, petrophysically distinct, onlapping slope layers	Petrophysical complexity within slope deposits	Seismic data from Browse Basin, NW Australia (Rankey, personal communication) Quaternary slope deposits, Maldives (Betzler et al., 2016)
Three Layer Offlapping	Three stacked, petrophysically distinct, offlapping slope layers	Petrophysical complexity within slope deposits Complex geometric relationships between slope bodies	Seismic data of Miocene isolated carbonate platforms, Browse Basin, NW Australia (Van Tuyl et al., 2018) Quaternary deposits, Maldives (Betzler et al., 2016)
Low-Relief Interfingering	More complex platform and slope geometries than other models, with two tongues of sediment extending into the basin	Platform-basin relief Complex relationships between slope and basinal shale facies	Modification of forward stratigraphic modeling results (Granjeon, 2020)

Table 2: Summary of among-model variations in geological and petrophysical attributes, variables, and inspiration of each scenario in the Aggrading Carbonate Margin and Low-Relief Interfingering suite of models.

Model	Description	Variable(s) Tested	Inspiration/Examples
Base	Control model. Prograding margin with no alteration to facies petrophysical properties	N/A	Central Luconia seismic data, (Kosa et al., 2015) Seismic data, Browse Basin, NW Australia; (Roesleff-Soerensen et al., 2012; Van Tuyl et al., 2018; Rankey, personal communication)
Toe of Slope Lowstand	High-impedance interval in a portion of the reef facies and a body of low-impedance carbonate at the toe of slope	Complex geometric relationships between slope bodies Petrophysical complexity within reef deposits	Outcrop observations and figures of the Upper Miocene Cariatiz carbonate platform, SE Spain (Reolid et al., 2014)
Flooding Layers	High- and low-impedance intervals in the reef facies, and three high-impedance intervals (carbonate mud) onlapping slope deposits	Complex geometric relationships between slope bodies Petrophysical complexity within reef deposits	Inverse scenario of the Cariatiz Carbonate platform, SE Spain (Reolid et al., 2014)
Tight Cliniform	One cliniform wherein both reef and slope facies are high-impedance carbonate	Complex geometric relationships between slope and basinal (carbonate mud) deposits	Seismic data of the Cretaceous Shuaiba Formation, Abu Dhabi (Yose et al., 2006)

Table 3: Summary of the geological and petrophysical differences, variables tested, and inspiration/examples of each scenario in the Prograding Carbonate Margin suite of models.

Model	Description	Variable(s) Tested	Inspiration/Examples
High Impedance Interior	Carbonate margin which is both prograding and aggrading. Identical facies distributions between models Clinoform relief and gradient increase basinward as the shelf builds	Two different petrophysical scenarios. One of high-impedance (4500 m/s) platform interior facies, and one of low-impedance (3250 m/s) platform interior facies	Seismic data from Browse Basin, NW Australia (Rankey, personal communication) Porosity/impedance patterns of isolated carbonate platforms, Central Luconia, Malaysia (Epting, 1980; Vahrenkamp et al., 2004; Zampetti et al., 2004; Warrlich et al., 2010)
Low Impedance Interior			

Table 4: Summary of the geological and petrophysical differences, variables tested, and inspiration/examples of each scenario in the Combination Prograding and Aggrading Carbonate Margin suite of models.

Appendix 1: Illustrative Model Detailed Description

22 of the 39 total models generated in this experiment are particularly illustrative of the range of seismic character which can result from the range of modeled geologic scenarios.

Understanding both the changes in seismic character themselves and the causal geological factors is critical in applying models to the interpretation of real-world data.

1. Base Aggrading

Reflector 1 is a low-amplitude, horizontal, and continuous peak. To the left of the blue arrow amplitude increases and the reflector dips basinward, with period gradually increasing by a small increment up to the yellow arrow. To the right of the yellow arrow, the reflector develops into a doublet for a short interval and the “jumps” upwards and increases in amplitude and period. Amplitude and period remain constant from the “jump” to the edge of the model.

Within the shelf, reflector 1 tracks the top of the lowest cemented interval. The increase in amplitude is the result of greater contrast between the cemented interval and reef facies relative to the shelf interior-cemented interval interface. The “jump” to the right of the yellow arrow is the result of a facies change from reef to slope deposits along the base of the model. This interval, like the lower interval of the first model, is kept consistent through all models to negate any edge effects from altering seismic character of slope deposits.

Reflector 2 is a low-amplitude, horizontal, and continuous trough. Like reflector 1, it increases in amplitude approaching the blue arrow and begins to dip basinward. The onset of dip coincides with a decrease in amplitude and an increase in period approaching the blue arrow. Between the blue and yellow arrows, reflector period increases. At the yellow arrow period decreases and amplitude increases before reaching a maximum and decreasing, eventually terminating into the basin.

Within the shelf, reflector 2 tracks the bottom of the middle cemented interval, and the increase in amplitude towards the shelf margin comes from the greater impedance contrast between the cemented interval and the reef facies. The “jump” that the reflector makes marks a facies transition from reef/cemented facies to slope deposits, and the basinward portion of the reflector follows along the bottom of the slope deposits.

Reflector 3 is a low-amplitude and horizontal peak which runs parallel to overlying and underlying reflectors. Amplitude and period increase at the same point as reflectors 1 and 2, but amplitude and period decrease as it begins to dip basinward before combining with reflector 5 at the blue arrow. At the blue arrow and moving basinward, amplitude and period increase to relative maxima before amplitude begins to decrease before the reflector terminates in the basin.

Within the shelf, reflector 3 tracks the top of the middle cemented interval. The increase in amplitude comes from the increased impedance contrast between the cemented interval and reef facies. The decrease in amplitude and period before it amalgamated with reflector 5 resulted from a facies transition as the cemented interval terminated and the peak began following the top of slope deposits instead. Amplitude and period peak where slope deposits were the thickest before decreasing as the slope pinched out.

Reflector 4 is a moderate-amplitude, horizontal trough which runs parallel to overlying and underlying reflectors. It increases in amplitude and becomes concave down to the left of the blue arrow and terminates at the confluence of reflectors 3 and 5.

Reflector 4 tracks the bottom of the upper cemented interval. The increased amplitude relative to reflector 2 is the result of constructive interference from the basinal shale-top carbonate interface, and the reflector terminates where the cemented interval stops.

Reflector 5 is a high-amplitude and horizontal peak which runs parallel to reflector 4. To the left of the blue arrow, reflector amplitude increases and the reflector dips basinward. At the blue arrow, amplitude decreases, and period increases as reflectors 3 and 5 combine.

Reflector 5 tracks the top of the shelf (top carbonate) all the way through the model. The loss of amplitude and increase in period at the blue arrow results from a facies change.

2. *Onlapping 3 Layers*

Reflector 1 is a low-amplitude, horizontal, and continuous peak. To the left of the blue arrow amplitude increases and the reflector dips basinward, with period gradually increasing by a small increment up to the yellow arrow. To the right of the yellow arrow, the reflector develops into a doublet for a short interval and the “jumps” upwards and increases in amplitude and period. Amplitude and period remain constant from the “jump” to the edge of the model.

Within the shelf, reflector 1 tracks the top of the lowest cemented interval. The increase in amplitude is the result of greater contrast between the cemented interval and reef facies relative to the shelf interior-cemented interval interface. The “jump” to the right of the yellow arrow is the result of a facies change from reef to slope deposits along the base of the model. This interval, like the lower interval of the first model, is kept consistent through all models to negate any edge effects from altering seismic character of slope deposits.

Reflector 2 is a low-amplitude, horizontal, and continuous trough. Like reflector 1, it increases in amplitude approaching the blue arrow and begins to dip basinward. The onset of dip coincides with a decrease in amplitude and an increase in period approaching the blue arrow. Between the blue and yellow arrows, amplitude decreases while period increases. At the yellow arrow, the reflector “jumps” at which point amplitude increases and period decreases while the

reflector remains dipping basinward. Amplitude peaks before gradually decreasing while period remains consistent before the reflector terminates at the edge of the model.

Within the shelf, reflector 2 tracks the bottom of the middle cemented interval, and the increase in amplitude towards the shelf margin comes from the greater impedance contrast between the cemented interval and the reef facies. The “jump” that the reflector makes marks a facies transition from reef/cemented facies to slope deposits, and the basinward portion of the reflector follows along the bottom of the slope deposits before eventually transitioning to be a part of the sidelobe of reflector 1.

Reflector 3 is a low-amplitude and horizontal peak which runs parallel to overlying and underlying reflectors. Amplitude and period increase at the same point as reflectors 1 and 2, but amplitude and period decrease as it begins to dip basinward before combining with reflector 5 at the blue arrow. At the blue arrow and moving basinward, amplitude and period increase to relative maxima before amplitude begins to decrease before the reflector terminates in the basin.

Within the shelf, reflector 3 tracks the top of the middle cemented interval. The increase in amplitude comes from the increased impedance contrast between the cemented interval and reef facies. The decrease in amplitude and period before it amalgamated with reflector 5 resulted from a facies transition as the cemented interval terminated and the peak began following the top of slope deposits instead. Amplitude and period peak where slope deposits were the thickest before decreasing as the slope pinched out.

Reflector 4 is a moderate-amplitude, horizontal trough which runs parallel to overlying and underlying reflectors. It increases in amplitude and becomes concave down to the left of the blue arrow and terminates at the confluence of reflectors 3 and 5.

Reflector 4 tracks the bottom of the upper cemented interval. The increased amplitude relative to reflector 2 is the result of constructive interference from the basinal shale-top carbonate interface, and the reflector terminates where the cemented interval stops.

Reflector 5 is a high-amplitude and horizontal peak which runs parallel to reflector 4. To the left of the blue arrow, reflector amplitude increases and the reflector dips basinward. At the blue arrow, amplitude decreases, and period increases as reflectors 3 and 5 combine.

Reflector 5 tracks the top of the shelf (top carbonate) all the way through the model. The loss of amplitude and increase in period at the blue arrow results from a facies change.

3. *Prograding Base Model*

Reflector 1 is a high-amplitude, horizontal to undulatory and continuous peak which is partially truncated due to model edge effects. From left to right reflector rises approximately 20 ms while gradually losing amplitude and maintaining a constant period before terminating against the bottom of the model and reflector 2.

Reflector 1 follows the slope-carbonate mud interface across the entire model, and it climbs from left to right because the slope-mud interface gradually rises in the section across the model before it gets washed out by reflector 2.

Reflector 2 is a moderate-amplitude, horizontal, and continuous trough. It starts as a doublet before the two troughs gradually combine into a single wiggle trace (decrease in period) with no change in amplitude. Towards the right edge of the model, the reflector begins dipping basinward and increases in amplitude before terminating at the edge of the model.

Reflector 2 is likely a combination of a sidelobe of the basinal shale-reef interface and the actual reef-slope trough, which partially explains why it initially manifests as a doublet on the left portion of the model. The doubled amalgamates into a single trough where reef facies get

thinner. The change in character towards the right edge of the model mark where reflector 2 becomes a sidelobe of the top carbonate reflector and impedance contrast between carbonate and shale increases.

Reflector 3 is a high-amplitude, horizontal, and continuous peak. Reflector 3 dips basinward at a very low angle for most of the lateral extent of the model, sinking about 10 ms. Towards the edge of the model, reflector dip angle increases as does amplitude before the reflector reaches the edge of the model.

Reflector 3 is top carbonate across the entirety of the model. The change in character towards the right edge of the model marks the reef-slope transition and increasing acoustic impedance further away from the shelf margin.

4. *Prograding Toe of Slope Lowstand*

Reflector 1 is a low-amplitude, horizontal, and continuous peak which runs parallel to overlying reflectors. Amplitude and period remain consistent up to the yellow arrow, though the lower portion of each “wiggle” is truncated due to edge effects from the depth-to-time conversion. At the yellow arrow, reflector 1 rises in TWT, increases in amplitude decreases in period, and dips basinward at a very low angle before terminating against the model’s edge.

Within the shelf, reflector 1 is the product of impedance contrasts between clinoforms within the slope in addition to the sidelobe of the impedance contrast traced by reflector 2. It increases in amplitude at the yellow arrow as the result of constructive interference from the increase in reflector 2’s amplitude caused by the lowstand deposits.

Reflector 2 is moderate-amplitude, dominantly horizontal, and continuous trough. Amplitude increases and period remains the same at the blue arrow. Approximately halfway through the portion of increased amplitude, period decreases for a short interval. The remaining span of the

reflector prior to the yellow arrow decreases in amplitude and increases in period. At the yellow arrow, amplitude increases for the 2nd time while period decreases. The 2nd span of increased amplitude ends towards the edge of the model where amplitude and period decrease and the reflector dips basinward before terminating at the edge of the model.

Within the shelf, reflector 2 traces the reef-slope facies interface. The two intervals of increased amplitude coincide with the cemented interval in the reef and lowstand debrites respectively.

Reflector 3 is a high-amplitude, dominantly horizontal, and continuous trough with variable amplitude which runs parallel to reflector 2. At the blue arrow reflector amplitude increases and period decreases for a limited portion of the reflector. Amplitude then decreases up to the yellow arrow, at which point period and amplitude increase. At the edge of the model, the reflector dips basinward while amplitude increases until the reflector terminates at the model's edge.

Reflector 3 tracks the top of carbonate, and the amplitude increase at the blue arrow is the result of the cemented interval within the reef. Small, insignificant changes in amplitude and period are caused by the shape of the basin shale-reef interface. The point where dip angle and amplitude increase marks the extent of the shelf and the amplitude increase is the result of increasing slope impedance values moving away from the shelf margin.

5. Prograding with Flooding Intervals and Cemented/Porous Reef Facies

Reflector 1 is a moderate-amplitude, sub-horizontal, and continuous reflector which runs parallel to reflector 2a and 2b. Towards the middle of the model, reflector 1's amplitude decreases, and it climbs approximately 20 ms. It then dips basinward beneath reflector 2b and terminates at the base of the model and reflector 2b.

Reflector 1 follows the base of the carbonate slope clinoforms and tracks their interface with carbonate mud. The point at the middle of the model where its “climbs” follows where the slope-mud interface is higher in the section. The reflector terminates due to destructive interference from reflector 2b.

Reflector 2 is a moderate-amplitude, sub-horizontal, and continuous reflector. It's first segment, 2a, increases to high-amplitude several traces into the model, dipping slightly basinward. Approximately one-third of the way across the model, the high-amplitude segment ends and reflector 2a decreases to moderate and then to low-amplitudes with increased period before terminating for a several traces. Reflector 2 reappears as reflector 2b, a low-amplitude, basinward dipping reflector which increases in amplitude and period before terminating at the edge of the model.

Reflectors 2a and 2b trace the reef-slope interface across the entirety of the shelf, before reflector 2b becomes a sidelobe of the top carbonate reflector at the edge of the model. The high-amplitude portion of reflector 2a aligns with the cemented carbonate in the reef, and the lower-amplitude higher-period interval tracks the reef-slope interface that has a smaller impedance contrast. The interruption in reflector 2, marking the transition to 2b, coincides with the high-porosity low-impedance carbonate portion of the reef facies. 2b again follows the reef-slope interface before transitioning to be a sidelobe of the top carbonate reflector at the far edge of the model.

Reflector 3 is a moderate-amplitude, sub-horizontal, and continuous reflector. After a short interval, it increases to be high-amplitude and slightly basinward dipping. Approximately one-third of the way across the model, amplitude decreases back to moderate values. Coinciding with reflector 2's discontinuity, the reflector drops approximately 15 ms and before rising back to the

original TWT depth of around 20 ms. The reflector then continues as a horizontal reflector until the final portion of the model, where it dips basinward, increasing in amplitude before terminating at the edge of the model.

Reflector 3 follows top-carbonate across the entire model. The high-amplitude zone in the left side of the model coincides with the cemented reef zone, and the “dip” interval in the right one-third of the model coincides with the low-impedance carbonate in the reef. The basinward dipping portion marks the transition from reef to slope facies interfacing with basinal shale, and the increase in amplitude is due to increasing mud content and decreasing porosity moving further from the shelf margin.

6. *Prograding with a High-Impedance LST/TST Clinoform*

Reflector 1 is a moderate-amplitude, concave-down (due to edge effects from the time-depth conversion) peak which terminates against the base of the model and reflector 2.

Reflector 1 marks the slope-carbonate mud interface and is terminated by the effects of other slope clinoforms.

Reflector 2 is a high-amplitude, basinward-dipping trough which rapidly decreases in amplitude before terminating at the edge of the model.

Reflector 2 follows the base of the tight clinoform and loses amplitude as the tight carbonate thins out.

Reflector 3 is a high-amplitude, basinward dipping and continuous peak. At the position where reflectors 4 and 5 onlap, it decreases in amplitude and period while dip angle increases. The reflector then terminates due to loss of amplitude before reaching the base of the model.

Reflector 3 follows the top of the tight clinoform in the model, and the change in character where reflectors 4 and 5 onlap are likely mostly due to decreasing thickness of the tight clinoform.

Reflector 4 onlaps reflector 3 several traces to the right of where reflector 5 onlaps/diverges from reflector 3. It is a moderate-amplitude, basinward-dipping and continuous trough which has an increase in amplitude and period towards the right edge of the model, where it begins to dip more steeply.

Reflector 4 is the reef-slope interface and onlaps reflector 3 because the reef/slope deposits onlap the tight clinoform. The change in geometry and increase in amplitude and period towards the rightmost edge of the model coincides with reflector 4 becoming a sidelobe of top carbonate.

Reflector 5 onlaps or diverges from reflector 3 towards the edge of the model. It is a moderate-amplitude, horizontal to sub-horizontal peak. Towards the right edge of the model, the reflector dips basinward and increases in amplitude before reaching the edge of the model.

Reflector 5 marks top carbonate basinward of the tight clinoform. The change in character towards the edge of the model comes from the transition from reef to slope facies interfacing with basinal shale, and the associated increase in acoustic impedance moving away from the shelf margin.

7. Aggrading with High Acoustic Impedance Shelf Interior Facies

Reflector 1 is a moderate-amplitude, horizontal, and continuous peak running parallel to all overlying reflectors. Amplitude decreases basinward before terminating against reflector 2 at the blue arrow.

Reflector 1 is a sidelobe of the trough from the reef-slope interface, and the basinward decrease in amplitude is due to destructive interference from the mud-slope interface.

Reflector 2 is a moderate-amplitude, horizontal, and continuous trough which runs parallel to overlying reflectors. Reflector period decreases basinward, while amplitude reaches a maximum in the middle of the model before beginning to decrease approaching the blue arrow. At the blue arrow, period decreases while amplitude remains constant and the reflector dips basinward and terminating against the bottom of the model.

Within the shelf, reflector 2 follows the reef-slope interface. The increase in amplitude in the middle of the shelf and subsequent decrease in amplitude and period are tied to constructive interference with the sidelobe of reflector 3. At the blue arrow reflector 2 is only the sidelobe of the top carbonate reflector.

Reflector 3 is a high-amplitude, horizontal, and continuous peak which runs parallel to underlying and overlying reflectors. It shows a basinward decrease in amplitude while period stays constant approaching the blue arrow. At the blue arrow, the reflector dips basinward. Amplitude increases while period decreases over a short interval before increasing basinward and the reflector then terminates at the edge of the model.

Reflector 3 tracks top carbonate for the duration of the model. The decrease in amplitude towards the blue arrow is due to the thinning out of shelf facies which has a greater impedance contrast with basinal shale than reef facies. The blue arrow marks the shelf margin, and the basinward increase in amplitude is caused by increasing acoustic impedance as slope facies gradually become muddier with increasing distance from the shelf margin.

Reflector 4 is a moderate-amplitude, horizontal, and continuous trough which runs parallel with reflector 3. Reflector amplitude decreases approaching the blue arrow. At the blue arrow, amplitude begins to increase while period decreases for a short interval before increasing

basinward. The reflector returns to horizontality in the basin and terminates at the edge of the model.

Reflector 4 is a sidelobe for the top carbonate reflector, hence patterns in its amplitude, period, and geometry mimic that of reflector 3.

8. *Aggrading with Low Acoustic Impedance Shelf Interior Facies*

Reflector 1 is a moderate-amplitude, shelfward dipping, and continuous peak which runs parallel to overlying reflectors. Amplitude decreases approaching the blue arrow, at which point reflector 2 truncates reflector 1.

Geologically, reflector 1 is a side lobe peak of reflector 2, which itself follows the reef-slope interface.

Reflector 2 is a moderate-amplitude, initially shelfward dipping, and continuous trough. To the right of the model's edge, reflector period rapidly decreases and amplitude increases. After that point, period increases while amplitude remains consistent moving towards the blue arrow. To the left of the blue arrow, the reflector turns horizontal for a small interval before dipping basinward at the blue arrow. Coinciding with the change and dip direction is a decrease in period. Finally, reflector 2 terminates against the model base with the final several traces increases in amplitude.

Within the shelf, reflector 2 tracks the reef-slope interface. The rapid decrease in period in the far-left portion of the reflector is a function of how the model was drawn, and does not represent anything geologically significant. The change in dip direction from shelfward to basinward at the blue arrow denotes where the reflector ceases tracking the reef-slope interface and is instead the sidelobe for the top carbonate reflector (reflector 3).

Reflector 3 is a moderate-amplitude, shelfward dipping, and continuous peak which runs parallel to underlying and overlying reflectors. In the middle of the model, reflector amplitude decreases for a short interval before it increases approaching the blue arrow. At the blue arrow, reflector 3 dips basinward and amplitude and period begin to increase before the reflector reaches horizontality and terminates at the edge of the model.

Within the shelf, reflector 3 tracks the shelf interior-reef interface. The increase in amplitude approaching the blue arrow is a result of the shelf interior facies pinching out and the reef facies, which in this model has much higher acoustic impedance values than interior facies and thus higher impedance contrast and greater reflector amplitude. Starting slightly to the left of the blue arrow and continuing basinward, reflector 3 tracks the top carbonate from reef to slope, and increasing amplitude and period are a product of increased impedance moving away from the margin and less destructive interference within the resolution of the 22 Hz wavelet.

Reflector 4 is a moderate-amplitude, shelfward dipping, and continuous trough which runs parallel to underlying and overlying reflectors. It shows basinward decreases in amplitude and period, overlapping reflector 3 approximately one-third of the way across the model.

Reflector 4 is the result of constructive interference between the sidelobes of top carbonate and the shelf interior-reef interface. It terminates as shelf interior facies thin out and constructive interference turns into destructive interference.

Reflector 5 is a low-amplitude, horizontal, and continuous peak which runs parallel to reflector 4. It decreases in amplitude and period before terminating at the same point as reflector 4, approximately one-third of the way across the width of the model.

Reflector 5 marks the top of the shelf at the shelf interior-basin shale interface. It loses amplitude and period before terminating due to destructive interference as shelf interior facies thin out below seismic resolution.